Preprint typeset in JHEP style - PAPER VERSION

JHEP **11** (2004) 009

Photon tagged correlations in heavy ion collisions

F. Arleo [a,b], **P. Aurenche** [c], **Z. Belghobsi** [c,d], **J.-Ph. Guillet** [c]

[a] *Université de Liège, Institut de Physique B5, Sart Tilman, 4000 Liège 1, Belgique*

[b] *LPTHE *, Université Paris VI & Paris VII et CNRS, 4, Place Jussieu, 75252 Paris cedex 05, France*

[c] *LAPTH †, B.P.110, 74941 Annecy-le-Vieux cedex, France*

[d] *Laboratoire de Physique Théorique, Université de Jijel, B.P. 98, Ouled Aissa, 18000 Jijel, Algérie*

E-mail: arleo@lpthe.jussieu.fr, aurenche@lapp.in2p3.fr, belghob@lapp.in2p3.fr, guillet@lapp.in2p3.fr

Abstract: A detailed study of various two-particle correlation functions involving photons and neutral pions is presented in proton-proton and lead-lead collisions at the LHC energy. The aim is to use these correlation functions to quantify the effect of the medium (in lead-lead collisions) on the jet decay properties. The calculations are carried out at the leading order in QCD but the next-to-leading order corrections are also discussed. The competition between different production mechanisms makes the connection between the jet energy loss spectrum and the $\gamma-\pi^0$ correlations somewhat indirect while the $\gamma-\gamma$ correlations have a clearer relation to the jet fragmentation properties.

Keywords: QCD, Jets, Hadronic Colliders.

*UMR 7589 du CNRS

†UMR 5108 du CNRS, associée à l'Université de Savoie

Contents

1. Introduction

Electromagnetic probes have long been thought to be useful to detect the formation of a quark-gluon plasma in ultrarelativistic heavy ion collisions [1, 2, 3, 4]. Many observables involving photons can in principle be used. One of the simplest, from a theoretical point of view, is the single photon spectrum as a function of the transverse momentum $p_{_T}$: it is expected that secondary collisions in heavy ion scattering will produce an excess of direct photons, as compared to proton-proton scattering, in an energy domain a few times the plasma temperature. However the flux of background photons from hadronic resonances is quite large and this makes the extraction of

the direct photon signal a non trivial task experimentally. These observables would probe the plasma at the early times of the collision when the medium is the hottest.

Photons can also be used in a different kinematical regime, namely at large transverse momentum (many times the temperature of the plasma). Such photons are produced in primary collisions *i.e.* as in proton-proton collisions and, ideally, their production rate is calculable in perturbative QCD in the next-to-leading order (NLO) approximation [5]. For a high enough transverse momentum these direct photons should be easily extracted from the background since the ratio γ/π^0 is rapidly increasing with $p_{_T}$. One can then study the decay properties of the jet recoiling from the photon by considering various photon-hadron or photon-photon correlation functions where the hadron or the second photon are fragments of the jet [6, 7, 8]. In the simplest case, when the transverse momentum of the recoiling jet exactly balances that of the photon, such observables allow to map out the fragmention function of the jet traversing the medium [9]. For a sample of data large enough one hopes to study the difference in the shape of the fragmentation functions in proton-proton and ion-ion collisions. Of course the real situation is more complicated because the large $p_{_T}$ photon can itself be produced by bremsstrahlung [10] in which case the photon and the jet momenta become somewhat uncorrelated as it is also the case when higher order corrections are taken into account. Furthermore, in order to have a reasonable counting rate for the correlation studies one cannot consider photons with too large transverse momenta and the π^0 background may then remain a problem. Thus if one studies $\gamma - \pi^0$ correlations, the $\pi^0 - \pi^0$ contribution should also be considered in turn.

In the following we will study various $\gamma-\gamma$, $\gamma-\pi^0$ and $\pi^0-\pi^0$ correlations both in proton-proton and lead-lead collisions at the LHC. Shadowing effects will be considered and, following standard practice, we will assume that the effects on the hard process of the parton multiple scattering through the medium can be parametrized by a modification of the fragmentation functions. The results are obtained in the leading-logarithm approximation of QCD since the status of NLO calculations in a medium is not yet clear. Our results should therefore be considered only as semi-quantitative. The model will be presented in the next section with special emphasis on the medium modified fragmentation effects. Then we turn to several observables and compare their behavior in proton-proton and lead-lead collisions. A discussion of the effects of NLO corrections in proton-proton collisions is given specifically to test the stability of the shape of observables. We consider this to be indicative of the stability of correlations under higher order corrections in heavy ion collisions.

2. The model

2.1 The leading order cross section

At the leading order in QCD the basic two-particle correlation cross-section, from which we will construct various observables, can be written [6]

$$\frac{d\sigma^{AB\to CD}}{dp_{T3}dy_3dz_3dp_{T4}dy_4dz_4} = \frac{1}{8\pi s^2}\sum_{a,b,c,d}\frac{D_{C/c}(z_3,M_F)}{z_3}\frac{D_{D/d}(z_4,M_F)}{z_4}\,k_{T3}\,\delta(k_{T3}-k_{T4}) \\ \frac{F_{a/A}(x_1,M)}{x_1}\,\frac{F_{b/B}(x_2,M)}{x_2}\,|\overline{M}|^2_{ab\to cd} \qquad (2.1)$$

where p_{Ti} and y_i, $i = 3, 4$, are respectively the transverse momenta and rapidities of the final state particles. The momentum k_{Ti}, $i = 3, 4$, is the transverse momentum of the parton c (respectively, d) which emits particle C (respectively, D) of momentum p_{Ti}, carrying a fraction $z_i = p_{Ti}/k_{Ti}$ of the parton momentum. The fragmentation functions $D_{C/c}$ and $D_{D/d}$ depend on the collinear factorization scale M_F. For the production of hadrons we will use the leading order functions of [11]. When a photon is detected in the final state it can be either produced directly, in which case the fragmentation function $D_{\gamma/c}(z, M_F)$ reduces to a Dirac function $\delta(1-z)$ or it can be produced via bremsstrahlung of a final state quark or gluon (see Figure 1 for illustration). In the latter case we use the BFG parametrization[1] of [12]. The structure functions $F_{a/A}$ and $F_{b/B}$ of the projectile and target, A and B, depend on the factorization scale M and they are normalized to one nucleon. Our standard in the following study is the parametrization of CTEQ6L [13].

The quantity $|\overline{M}|^2_{ab\to cd}$ is the matrix element squared, averaged over spin and color, of the partonic sub-process $ab \to cd$. It depends implicitely on the renormalisation scale μ through the strong coupling $\alpha_s(\mu)$. In the following, unless otherwise specified, all scales, μ, M, and M_F, are set equal to $(p_{T_3} + p_{T_4})/2$. Higher order corrections to Eq. (2.1) have been calculated and extensive phenomenological studies have been made in the case of proton-proton collisions [6, 7, 8, 14, 15, 16]. They are briefly discussed in Section 6.

2.2 Initial state nuclear effects

The structure function of a nucleon in a nucleus is modified by shadowing and anti-shadowing effects. These effects are hard to calculate theoretically and in this study we will simply use a parametrization of the parton distribution functions measured in deep-inelastic scattering experiments of leptons off nuclei [17] and Drell-Yan production in proton-nucleus reactions [18]. We follow the approach of Eskola *et al.* [19] who

[1] These parametrizations are given at the NLO of QCD. Nevertheless we use them for our leading-logarithmic studies for lack of recent leading-logarithmic parametrizations.

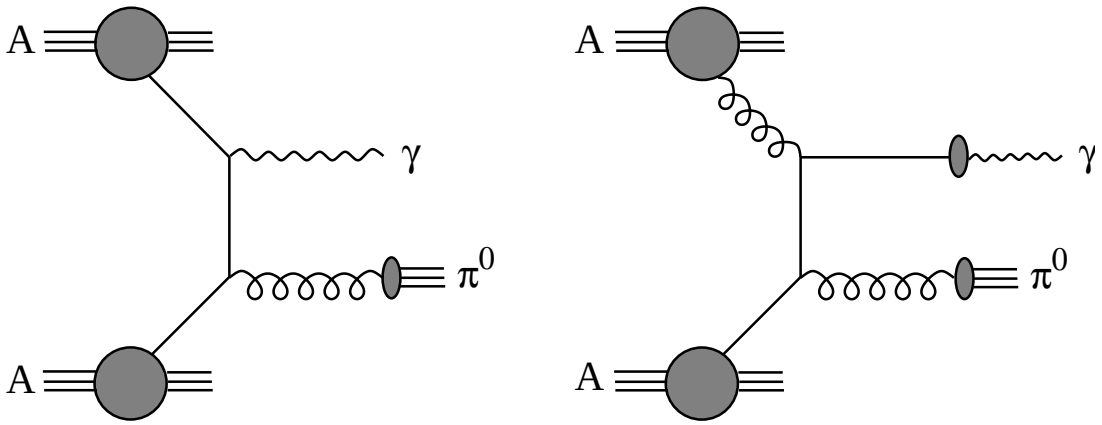

Figure 1: Two processes which contribute to $\gamma - \pi^0$ production at leading order: the photon may be produced directly (one-fragmentation, labeled 1f in the text, *left*) or by parton fragmentation (two-fragmentation, labeled 2f, *right*).

tabulate a function $S_{a/\mathrm{A}}(x, M)$ which relates the parton distributions in a nucleon N to those in a nucleus A via

$$F_{a/\mathrm{A}}(x, M) = S_{a/\mathrm{A}}(x, M)\, F_{a/N}(x, M) \tag{2.2}$$

Unlike older parametrizations, it is to be noted that the parametrization of [19] treats quarks and gluons separately and, furthermore, the factorization scale dependence is taken into account. In this parametrization, shadowing effects reduce the quark (by up to 10%) and the gluon (by up to 30%) distributions in the nucleon below $x \lesssim 0.03$, while anti-shadowing enhances the distributions by up to 10% between[2] $x = 0.03$ and $x = 0.4$. Since observables usually involve an integration over a rather large range in x, such shadowing/antishadowing effects will not affect the predictions very much. A summary of recent shadowing studies at LHC can be found in [20].

Plugging Eq. (2.2) in Eq. (2.1), with proper account of isospin effects, one obtains the cross section normalized per one nucleon in a nucleus. To obtain the counting rate in an actual heavy ion experiment one needs to account for the number of nucleon-nucleon scatterings occuring in a nucleus-nucleus collision. This is done in a standard way using Glauber theory. A hard cross section for an AA collision, with a given centrality class $\mathcal{C}$ (equivalently impact parameter range), is obtained from the corresponding hard cross section via the "binary scaling" relation

$$\sigma_{AA}^{hard}|_{\mathcal{C}} = \langle N_{coll} \rangle|_{\mathcal{C}}\, \frac{\sigma_{AA}^{geo}}{\sigma_{NN}}\, \sigma_{NN}^{hard} \tag{2.3}$$

where $\langle N_{coll} \rangle|_{\mathcal{C}}$ is the number of collisions at the chosen centrality, σ_{AA}^{geo} is the geometric cross section obtained via the Glauber multiple scattering model and σ_{NN} is the

[2]The precise x values depend on the factorization scale.

nucleon-nucleon cross section. Details, as well as the numerical values of the various terms, are given in [4]. In particular, for collisions with a centrality less than 5% the estimate is $\langle N_{coll} \rangle|_{\mathcal{C}} = 1876$ and $\sigma_{AA}^{geo} = 7745$ mb for lead-lead collisions at 5.5 TeV with $\sigma_{NN} = 72$ mb. In the following we implicitely consider only central collisions, with $\mathcal{C} \leq 5\%$, for lead-lead collisions. When quoting numbers of events for a given observable we assume the standard luminosity for lead-lead collisions in ALICE, $\mathcal{L} = 5.10^{26}$ cm^{-2} sec^{-1}, and make the hypothesis that LHC is running 30 days per year in the heavy ion mode.

2.3 Medium-modified fragmentation functions

Much progress has been done over the last decade to better understand the gluon radiation by hard partons travelling through dense QCD media [21]. More recently, the important connection between the medium-induced gluon spectra $dI/d\omega$ and the probability distribution $\mathcal{P}$ in the energy loss has been made explicit [22] and computed numerically soon after [23, 24]. However, it remains unclear how to relate the parton energy loss mechanism to observable quantities.

For sufficiently large $k_{_T}$ parton production, nevertheless, a clear separation is achieved between the hard production process, with a time scale $\mathcal{O}\left({k_{_T}}^{-1}\right)$, the effects of the medium, $\mathcal{O}\left(t_{\rm med}\right)$, and the fragmentation mechanism, $\mathcal{O}\left(k_{_T}/\Lambda^2\right)$,

$$\frac{1}{k_{_T}} \ll t_{\rm med} \ll \frac{k_{_T}}{\Lambda^2} \tag{2.4}$$

Provided the hierarchy (2.4) is justified, it is sensible to model the energy loss effects at the level of fragmentation functions. In the present study, we shall follow the model suggested in Ref. [9] in which the energy ϵ lost by the hard parton leads to a rescaling of the momentum fraction z_d

$$z_d = \frac{p_{_{Td}}}{k_{_{Td}}} \qquad \rightarrow \qquad z_d^* = \frac{p_{_{Td}}}{k_{_{Td}} - \epsilon} = \frac{z_d}{1 - \epsilon/k_{_{Td}}} \tag{2.5}$$

in presence of a QCD medium. Consequently, the medium-modified fragmentation functions $D_{D/d}^{\rm med}(z_d, M_{_F}, k_{_{Td}})$ may simply be expressed as a function of the standard (vacuum) fragmentation functions $D_{D/d}(z_d, Q^2)$,

$$z_d\, D_{D/d}^{\rm med}(z_d, M_{_F}, k_{_{Td}}) = \int_0^{k_{_{Td}}(1-z_d)} d\epsilon\ \mathcal{P}_d(\epsilon, k_{_{Td}})\ \ z_d^*\, D_{D/d}(z_d^*, M_{_F}). \tag{2.6}$$

Here, $\mathcal{P}_d(\epsilon, k_{_{Td}})$ denotes the probability for the parton with energy $k_{_{Td}}$ to lose the energy ϵ [22], which has been given a simple analytic parametrization in [23] which we shall use in the present calculations. The calculation of Ref. [23] is based on the medium-induced gluon spectrum determined by Baier, Dokshitzer, Mueller, Peigné and Schiff (BDMPS) including $\mathcal{O}\left(1/k_{_{Td}}\right)$ corrections [25, 26]. Such a model was shown to describe successfully hadron production in semi-inclusive DIS reactions off

nuclear targets [27]. The BDMPS framework should be particularly suited when the number of scatterings incurred by the hard parton in the QCD medium (opacity) is large. While thick and dense media are indeed expected to be produced in nuclear collisions at LHC energy, we note however that such a calculation may not properly describe the energy loss process for partons produced close to the surface. Let us mention that the probability distribution at *finite* opacity was also determined in the soft limit ($k_{_{Td}} \to \infty$) in Ref. [24] which lead to recent phenomenological applications at RHIC and LHC [28, 29].

The BDMPS energy loss distribution is characterized by the energy scale [25]

$$\omega_c = \frac{1}{2}\,\hat{q}\,L^2 \tag{2.7}$$

where the so-called gluon transport coefficient $\hat{q}$ reflects the medium gluon density [30] and L the length of matter covered by the hard parton in the medium. Note that $\hat{q}$ in (2.7) has to be seen as a time averaged quantity $\langle\hat{q}\rangle$ to take properly into account the longitudinal expansion of the produced medium [31].

For the calculations to come, a qualitative estimate of ω_c for the dense medium produced in lead-lead collisions at LHC energy is needed. The transport coefficient $\hat{q}$ is directly related to the gluon density whose increase from RHIC to LHC is of order $6-7$ in hydrodynamical calculations [28, 32], while a smaller increase $2-4$ in the hadron multiplicity at mid-rapidity (also linked to $\hat{q}$) is predicted by several models (a review can be found in [33]). Using the estimate based on the pion $p_{_T}$ spectra measurements at RHIC, $\omega_c|_{\rm RHIC} \simeq 10-20$ GeV, within the same framework [23, 34] we shall take throughout this study the rather conservative choice[3], $\omega_c = 50$ GeV.

Let us remind the reader that the goal here is not to provide quantitative predictions but rather to show typical trends one could expect in $\gamma-\gamma$ and $\gamma-\pi^0$ correlations in heavy-ion collisions at the LHC. Therefore, our conclusions should not depend much on the precise value we assume for the energy loss parameter ω_c.

Since fragmentation functions fall steeply with z, even a small shift $\Delta z_d = z_d^* - z_d \approx\ z_d\,\epsilon/k_{_{Td}}$ in Eq. (2.5) may substantially affect the fragmentation process due to parton energy loss. This can be seen for instance in Figure 2 where the fragmentation functions into a photon and into a neutral pion, using respectively the BFG [12] and KKP LO [11] parametrizations, are computed for $k_{_T} = 50$ GeV up quark and gluon traversing the medium ($\omega_c = 25, 50$ GeV) or not ($\omega_c = 0$ GeV).

First, Figure 2 indicates that medium effects prove stronger for gluon than for quark fragmentation. The origin is actually twofold. First, hard gluons lose more energy than quarks do from their larger color charge ($C_g = 3$, $C_q = 4/3$). Moreover, the quenching of medium-modified fragmentation functions Eq. (2.6) increases with

[3]This choice is motivated by the fact that the gluon distribution at very small x could evolve more slowly than seen so far at HERA due to possible gluon saturation. Moreover, we want our predictions to be seen as lower estimates as far as medium effects are concerned.

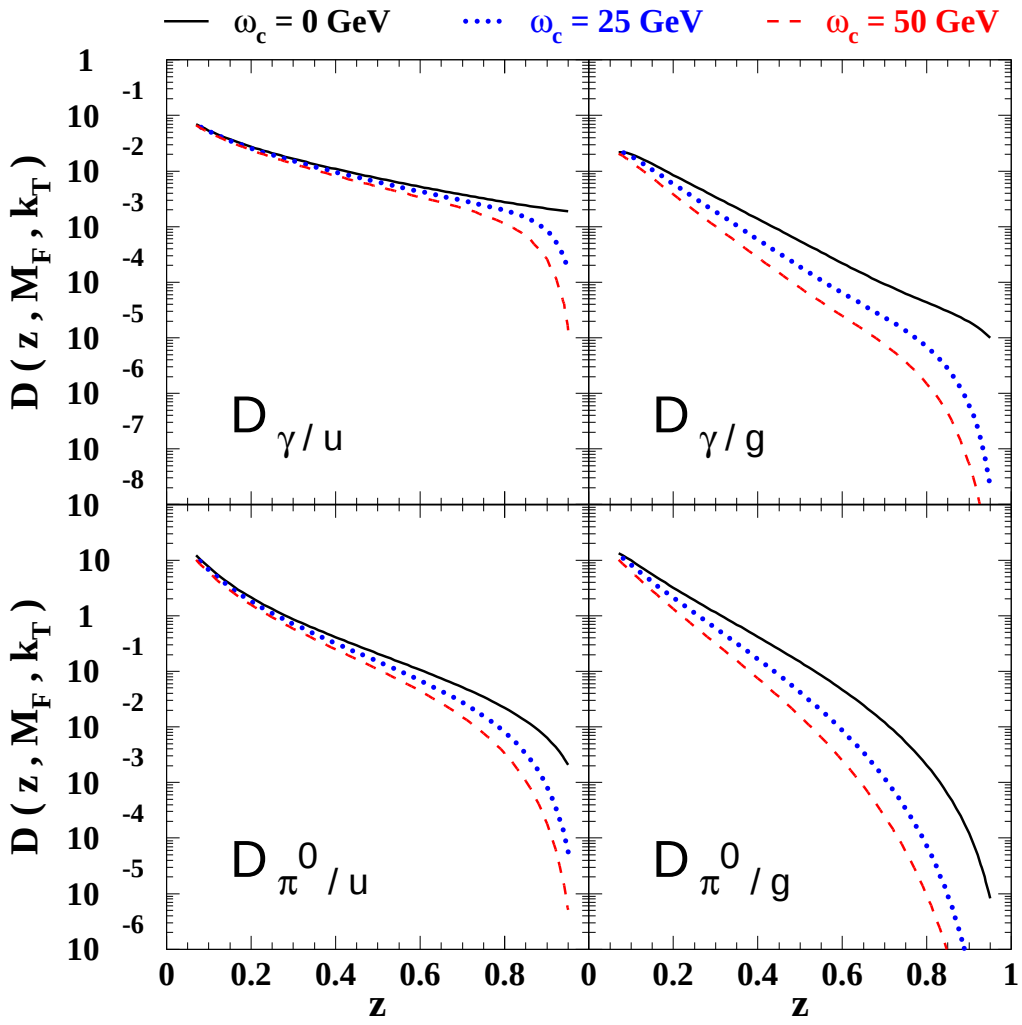

Figure 2: Medium-modified fragmentation functions $D^{\rm med}_{D/d}(z_d, M_{_F}, k_{_{Td}})$ for various energy loss scales, $\omega_c = 0$ (vacuum), 25 and 50 GeV. The parton energy is $k_{_T} = 50$ GeV and the fragmentation scale is set to $M_{_F} = p_{_T}/2$.

the slope of vacuum fragmentation functions, much steeper in the gluon channel. Finally, we observe that the effects of parton energy loss become more pronounced as z gets larger, due to the restricted available phase space in Eq. (2.6).

The medium-modified fragmentation functions depend now explicitely on the parton energy, $k_{_T}$. To show the sensitivity of the medium effects on the parton energy, the ratio of medium (using $\omega_c = 50$ GeV) over vacuum fragmentation functions is determined for $k_{_T} = 25, 50$ and 100 GeV quarks and gluons. As can be seen in Figure 3, medium effects will be magnified as the parton energy is getting smaller. When $k_{_T}$ becomes too small as compared to ω_c, however, the picture of a hard parton penetrating the soft medium is no longer correct and the applicability of the energy loss framework becomes doubtful. It was shown for instance in [23] that the

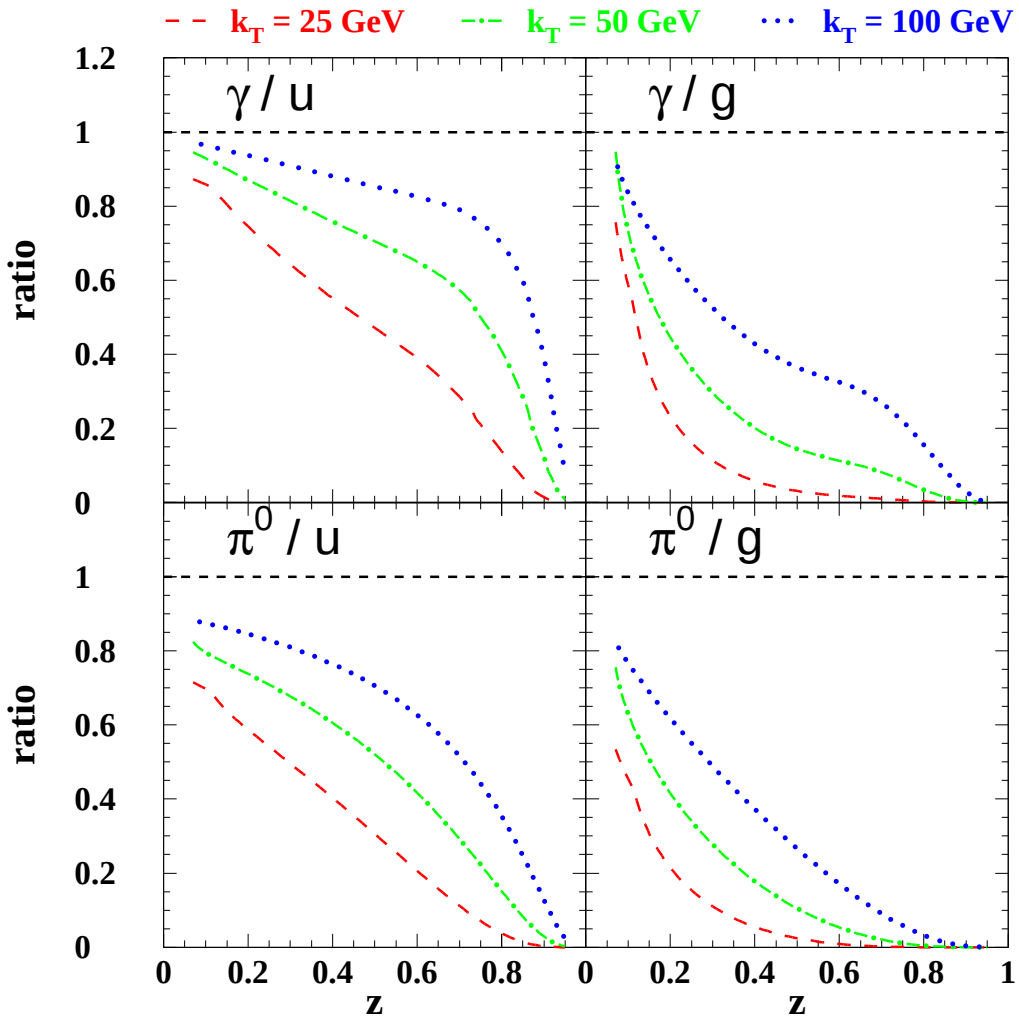

Figure 3: Ratio of medium-modified ($\omega_c = 50$ GeV) over vacuum ($\omega_c = 0$ GeV) fragmentation functions for various parton energy, $k_T = 25, 50$ and 100 GeV. The fragmentation scale is set to $M_F = p_T/2$.

eikonal approximation is explicitely broken down for parton energy smaller than half the scale ω_c. This has to be seen as the lower limit for the most energetic photon transverse momentum. On the other hand, in the high energy limit $k_T \gg \omega_c$ and thus $z^* \simeq z$, the medium effects vanish and the ratio approaches one.

3. The correlations

3.1 Observables

From the kinematical variables available in Eq. (2.1) we can construct the following observables:

– the invariant mass of the particle pair,

$$\begin{aligned} m_{34}^2 &= 2\ (p_{T3}p_{T4}\mathrm{ch}(y_3 - y_4) - \vec{p}_{T3} \cdot \vec{p}_{T4}) \\ &= 2\ z_3\ z_4\ k_T^2\ (\mathrm{ch}(y_3 - y_4) + 1) \end{aligned} \tag{3.1}$$

– the transverse momentum of the pair,

$$\begin{aligned} q_T &= |\vec{p}_{T3} + \vec{p}_{T4}| \\ &= k_T\ |z_3 - z_4| \end{aligned} \tag{3.2}$$

– the relative transverse momentum of the particles (also called momentum balance [6, 35])

$$\begin{aligned} z_{34} &= -\frac{\vec{p}_{T3} \cdot \vec{p}_{T4}}{p_{T3}^2} \\ &= \frac{z_4}{z_3} \end{aligned} \tag{3.3}$$

where k_T is the common value of the transverse momentum of the final state partons. For completeness we quote here the expressions of the x_i values of the initial partons,

$$\begin{aligned} x_1 &= \frac{1}{\sqrt{s}}\ \left(\frac{p_{T3}}{z_3}e^{y_3} + \frac{p_{T4}}{z_4}e^{y_4}\right) \\ x_2 &= \frac{1}{\sqrt{s}}\ \left(\frac{p_{T3}}{z_3}e^{-y_3} + \frac{p_{T4}}{z_4}e^{-y_4}\right) \end{aligned} \tag{3.4}$$

In the case of $\gamma - \pi^0$ correlations, one has $z_3 = 1$ when the photon is produced directly. Fixing furthermore the rapidity of the photon and the pion in a narrow range around 0, for example, we are left with two independent kinematical variables z_4 and k_T and the expressions of the observables defined above considerably simplify. One has:

$$\begin{aligned} m_{34}^2 &= 4\ k_T^2\ z_4 \\ q_T &= k_T\ |1 - z_4| \\ z_{34} &= z_4 \end{aligned} \tag{3.5}$$

which show a straightforward relation between the fragmentation variable z_4 and the observables.

When studying the observables we integrate over k_T above a given value. Since the cross section is rapidly falling when k_T is increasing the effective transverse momentum will remain close to its minimum value leaving z_4 as the only effective variable. From the behavior of the above observables one should get constraints on the behavior of the fragmentation function if we assume that the structure functions are precisely known.

When the photon is produced via bremsstrahlung or in the case of $\pi^0-\pi^0$ correlations the above simple situation is somewhat smeared because z_3 is now a relevant kinematical variable. However, when studying asymmetric configurations with a large p_{T3} particle on one side and a small p_{T4} particle on the other side, trigger bias effects will force a large value of z_3 and some correlation is still expected between the observables of Eqs. (3.1) to (3.3) and the z_4 dependent fragmentation function.

On the other hand, considering $\gamma - \gamma$ correlations, when both photons are produced directly, one has an over constrained system with $z_3 = z_4 = 1$ and the distributions in z_{34} and in q_T reduce to Dirac δ functions while the invariant mass $m_{34}^2 = 2k_T^2(\mathrm{ch}(y_3 - y_4) + 1)$ is regular. It is obvious that higher order corrections will smear the δ-function singularity. More precisely, $z_{34} = 1$, or equivalently $q_T = 0$, is an infrared sensitive point and an accurate prediction of the behavior of these observables near this point will require the resummation of large $\ln^2(q_T^2/s)$ and $\ln(q_T^2/s)$ terms.

3.2 Kinematical cuts

We study a basic perturbative QCD (pQCD) mechanism modified by the presence of a dense environment. It is necessary to insure that the particles we observe are decay fragments of jets and are not produced by secondary collisions. Recent studies [4] in the framework of perturbative QCD for primary collisions and a hydrodynamic model to describe secondary collisions have shown that, at LHC, particles produced above $p_T = 5$ GeV are of pQCD origin. We therefore impose a minimum transverse momentum of 5 GeV on the particles from which we construct the various correlation observables.

To study a large domain in the fragmentation variable z it is necessary to consider asymmetric configurations. Another constraint is to be able to distinguish photons from pions which requires, for ALICE for example, $p_{T_\gamma} > 25$ GeV. On the other hand, to have a reasonable counting rate, one should not go to too high values of p_{T_γ}. Besides, if jets are too energetic, energy loss effects will be small and difficult to observe.

In the subsequent studies, apart from various p_T distributions, we will look at the three distributions in Eqs. (3.1) to (3.3) with $p_{T_\gamma} > 25$ GeV and $p_{T_\pi} > 5$ GeV to satisfy the above criteria. We will also consider higher cuts in p_{T_γ} to probe the sensitivity of the energy loss mechanism on the jet energy. When displaying the distributions we always assume photons and pions are produced in an interval of $\delta y = \pm\, 0.5$ unit of rapidity around $y = 0$.

4. Phenomenology of $\gamma - \pi^0$ correlations

4.1 Dynamical components

Before studying the shape of correlation functions in lead-lead collisions it is worth-

while considering into some details the case of proton-proton scattering to better understand the dynamics of the reaction. As above mentioned (see Figure 1), the photon can be produced directly and only the recoiling jet fragments into a pion (labeled 1f, open squares in the following figures), or both the photon and the pion are produced by fragmentation of partons (labeled 2f, full squares).

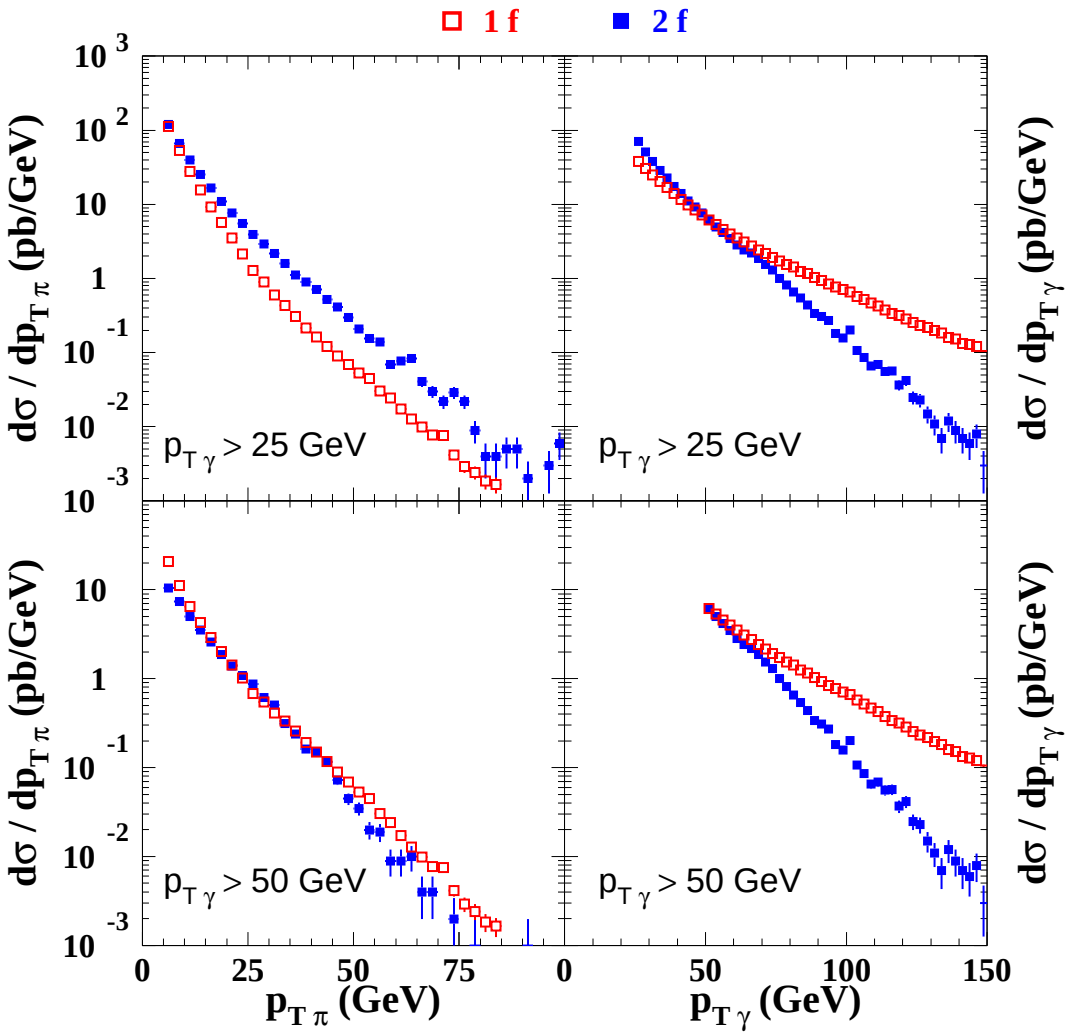

Figure 4: The 1f and 2f components for various kinematical configurations in $\gamma - \pi^0$ production for proton-proton scattering at $\sqrt{s} = 5.5$ TeV. *Top:* The p_{T_γ} and the p_{T_π} distributions for the cuts $p_{T_\gamma} > 25$ GeV and $p_{T_\pi} > 5$ GeV. *Bottom:* Same as above for $p_{T_\gamma} > 50$ GeV and $p_{T_\pi} > 5$ GeV.

The relative weight of each mechanism depends crucially on the transverse momentum of the produced particles. This is illustrated in Figure 4. On the right panels one displays the production rate as a function of p_{T_γ}: typically, the 2f process dominates when $p_{T_\gamma} < 50$ GeV but decreases much faster than the 1f component as p_{T_γ} increases and becomes negligible for photon transverse momenta above 100 GeV.

Therefore, changing the p_{T_γ} cut will affect dramatically the 1f and 2f relative contributions to $\gamma - \pi^0$ production.

As shown in Figure 4 (*left*), the pion p_{T_π} spectrum is dominated by the 2f process in a large p_{T_π} range when the photon energy is not too large ($p_{T_\gamma} \geq 25$ GeV) while applying a higher cut ($p_{T_\gamma} \geq 50$ GeV) in p_{T_γ} results into a comparable magnitude for both mechanisms on a wide p_{T_π} domain. Unlike the p_{T_γ} distribution the relative weight of the 2f process is increasing with the transverse momentum of the pion in the kinematical domain shown. Indeed, the 1f component is disfavored at large p_{T_π} as it requires more energetic photons ($p_{T_\gamma} \geq p_{T_\pi}$), while the 2f process allows the photon to keep a small transverse momentum, slightly above the 25 GeV or 50 GeV cut.

Experimentally, these two contributions may be disentangled by means of calorimetry techniques using appropriate isolation criteria. However, the large multiplicity reached in high energy heavy-ion collisions prevent one from using such techniques. It should also be reminded that when performing a full NLO study, the distinction between the leading-order fragmentation and the next-to-leading order direct component is arbitrary and depends on the fragmentation scale M_F, only the sum of these components being meaningful and ideally scale independent [7].

Medium effects may change considerably whether one or the other process dominates since the typical parton energy, $k_T = p_{T_\gamma}/z_3$, is quite different for 1f ($z_3 = 1$) and 2f ($z_3 < 1$). Naively, the effects of parton energy loss should be stronger when *both* the pion and the photon come from the hard parton fragmentation. However, this is not necessarily true since the parton energy is actually much greater in the 2f channel, for which medium effects prove weaker (see end of Section 2.3). We shall come back to these observations when discussing the proton-proton and lead-lead spectra in the next section.

4.2 Distributions

In Figure 5 we discuss four distributions, respectively in the pion transverse momentum p_{T_π}, the photon transverse momentum p_{T_γ}, the $\gamma - \pi^0$ invariant mass $m_{\pi\gamma}$ and the transverse momentum of the pair q_T. We impose the following cuts: $p_{T_\pi} \geq 5$ GeV and $p_{T_\gamma} \geq 25$ GeV. In each case three curves are displayed: proton-proton scattering (open dots), lead-lead scattering with shadowing but without energy loss (full squares) and lead-lead scattering with shadowing and energy loss using $\omega_c = 50$ GeV (open squares).

It is clear that shadowing and isospin effects do not modify the distributions very much: a small antishadowing effect can be observed at large transverse momenta or at high invariant mass due to the fact that the kinematics then becomes sensitive to larger x partons in the nuclei. Energy loss effects are quite visible particularly at the low p_T values of the pion or the photon. On the other hand, to produce a pion at high transverse momentum requires a parton with large k_T for which the energy loss is expected to be smaller. We observe, accordingly, that the spectrum in lead-lead

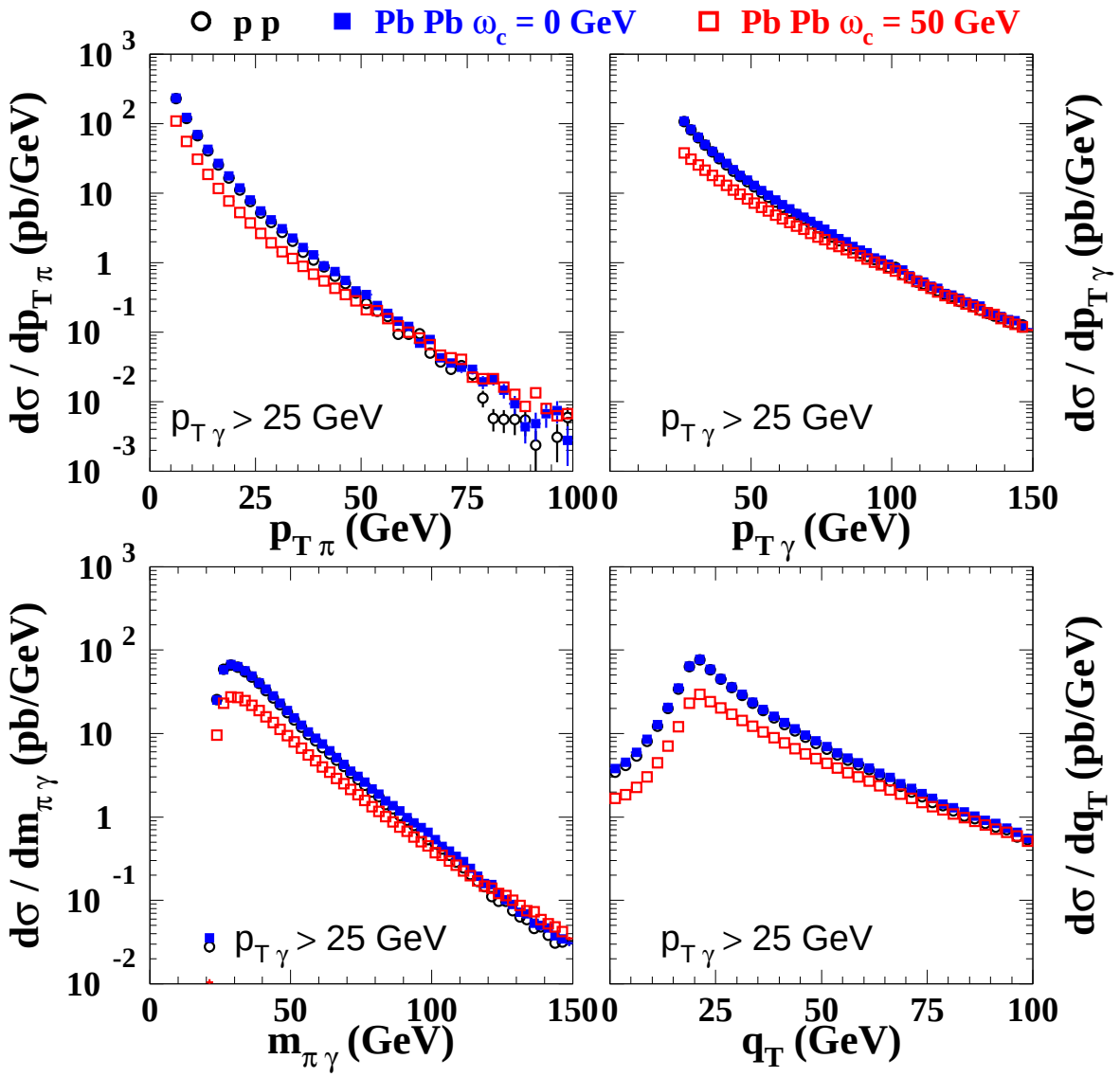

Figure 5: The four distributions in $\gamma - \pi^0$ production defined in the text for proton-proton (open dots) and lead-lead scattering (no energy loss: black squares; with energy loss: open squares) at $\sqrt{s} = 5.5$ TeV. Both the photon and the pion are produced at rapidity [-0.5, 0.5] and the following cuts are imposed: $p_{T_\gamma} > 25$ GeV and $p_{T_\pi} > 5$ GeV.

collision tends to approach the proton-proton spectrum as p_{T_π} increases. The medium effects are also particularly visible on the spectrum as a function p_{T_γ}: as long as the photon is produced directly (1f), the p_{T_γ} spectrum reflects the energy of the parton, $k_T = p_{T_\gamma}$, which eventually fragments into the pion. Again, the quenching will be maximal for small p_{T_γ} (small k_T) while at asymptotic energies, parton energy loss will have no observable consequence. Similar behavior is observed in the invariant mass distribution: small masses correspond to low k_T partons and therefore lead to a stronger suppression. One may notice, in passing, the rather large counting rates:

with the numbers given in Section 2.2 we estimate that about 1300 $\gamma - \pi^0$ pairs with a 100 GeV invariant mass will be produced, per year, in ALICE.

Perhaps, more interesting is the $q_{_T}$ spectrum which exhibits a maximum when the pion and the photon transverse momenta lie just above the imposed kinematic threshold, which is located at the difference between the $p_{_{T_\gamma}}$ and the $p_{_{T_\pi}}$ cut, 20 GeV. Above 20 GeV, the distribution is reminiscent of the $p_{_{T_\gamma}}$ and the $m_{\pi\gamma}$ distribution and, in particular, the larger the $q_{_T}$ the weaker the energy loss effect. Similarly, the energy loss effects will tend to be smaller at very small $q_{_T} \ll 20$ GeV as the pion transverse momentum and thus the 2f contribution – less affected by the medium – increases with decreasing $q_{_T}$. Therefore, we expect the medium effects to be maximal for $q_{_T}$ roughly around the difference of the transverse momentum cuts.

All these features are best seen when normalizing, to the proton-proton distributions, the lead-lead distributions with energy loss (open squares) or without energy loss (full squares) in Figure 6. In all cases it appears that the observables are affected by antishadowing, and not shadowing, but this remains a small effect, less than 10% in general. Energy loss effects, on the other hand, modify the distributions much more drastically. The $p_{_{T_\pi}}$ spectrum is suppressed by about 50% below $p_{_{T_\pi}} = 25$ GeV but no suppression occurs above 50 GeV. As for the $p_{_{T_\gamma}}$ distribution, the suppression is maximum at low transverse but is monotonously reduced as the momentum increases. In the $q_{_T}$ spectrum the change of slope discussed above it is particularly noticeable.

The same spectra are computed in Figure 7 assuming a larger cut for the photon transverse momentum, $p_{_{T_\gamma}} \geq 50$ GeV. Although the 1f contribution becomes relatively more important, one observes similar features as before. Again, the normalized $q_{_T}$ spectrum shows a clear minimum in Figure 8 around $q_{_T} \simeq 30$ GeV, under which the 2f contribution starts to dominate. The quenching of these spectra proves less pronounced – the ratio decreases down to 0.6 in the $q_{_T}$ spectra to be compared to 0.35 before – since the initial parton energy is twice as large. Finally, let us note that the counting rate drops by a factor 5 to 10 when increasing the photon cut from 25 GeV to 50 GeV.

We turn now to a detailed discussion of the distribution in the momentum balance $z_{_{34}}$ for both cuts $p_{_{T_\gamma}} \geq 25$ GeV and $p_{_{T_\gamma}} \geq 50$ GeV, keeping $p_{_{T_\pi}} \geq 5$ GeV as before (Figure 9, *top*). The maximum of these distributions is reached for $z_{_{34}} = 0.2$ and 0.1, i.e. the ratio of the pion over the photon transverse momentum cuts. Smaller (larger) $z_{_{34}}$ values are obtained by increasing the photon (pion) transverse momentum. Looking at the medium effects (Figure 9, *bottom*), one observes rather structureless features: as compared to the proton-proton case the spectrum is reduced to 40% (respectively 60%) over most of the $z_{_{34}}$ range when the cut $p_{_{T_\gamma}} > 25$ GeV (respectively $p_{_{T_\gamma}} > 50$ GeV) is imposed. Below $z_{_{34}} \leq 0.2$, the suppression is not as strong since the photon energy, hence $k_{_T}$, is getting larger.

We stressed in Section 3 that the momentum balance $z_{_{34}}$ is closely related to the

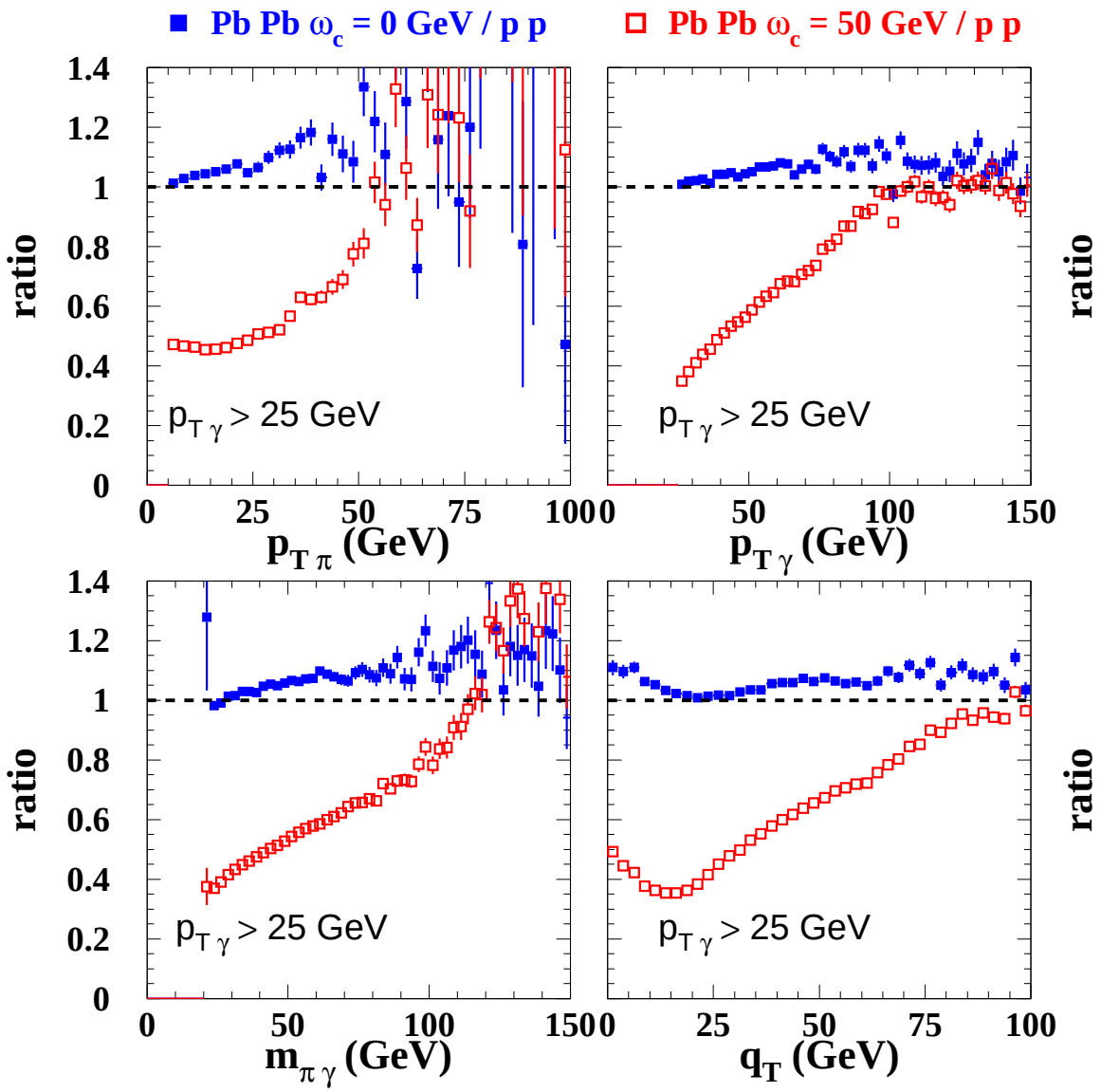

Figure 6: Same as Figure 5 but the distributions are normalized to proton-proton scattering.

fragmentation variable z when the photon is produced directly. Therefore, it may look surprising at first glance not to observe the suppression becoming more important when z_{34} gets close to one, as the ratio of medium over vacuum fragmentation functions may suggest in Figure 3. To understand the origin of the flat behavior of this ratio, the individual 1f and 2f contributions to the z_{34} distribution are represented in Figure 10 (*top*). When the p_{T_γ} cut is set to 25 GeV, most of the events (for $z_{34} > 0.15$) actually come from the double fragmentation process and the relative proportion of this 2f contribution increases with z_{34}. For this 2f component, however, the connection between the momentum balance and the fragmentation variable is lost. In particular, the pion transverse momentum gets larger as z_{34} increases, thereby

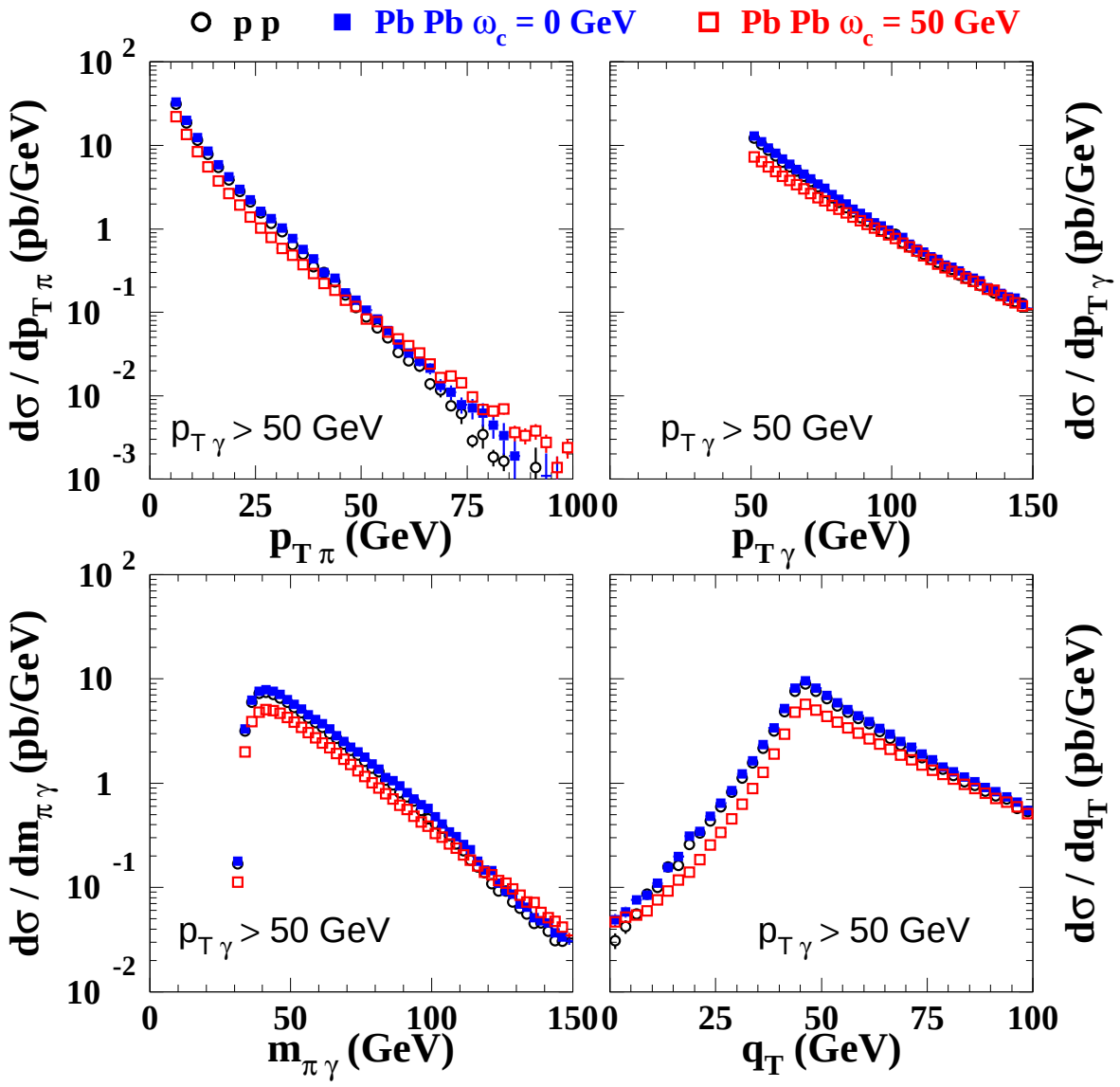

Figure 7: Same as Figure 5 with the following cuts: $p_{T_\gamma} > 50$ GeV and $p_{T_\pi} > 5$ GeV.

reducing the medium effects. To be more explicit, we show in the lower panel of Figure 10 the medium effects on the individual 1f (open squares) and 2f components (full squares) separately. As expected, the suppression in the 2f channel becomes less important when z_{34} increases unlike the 1f channel, whose suppression is reminiscent to the z dependence of the medium over vacuum fragmentation functions, with a vanishing ratio at $z_{34} \simeq 1$. Summing the two contributions, the resulting suppression (open circles) is an interplay between the 1f and 2f behavior. As far as counting rates are concerned they are rather large: for ALICE one expects about 5 10^5 pairs at $z_{34} = 0.5$ when $p_{T_\gamma} > 25$ GeV and 5 10^4 pairs when $p_{T_\gamma} > 50$ GeV.

In order to isolate the 1f channel – whose medium effect is remarkable – it

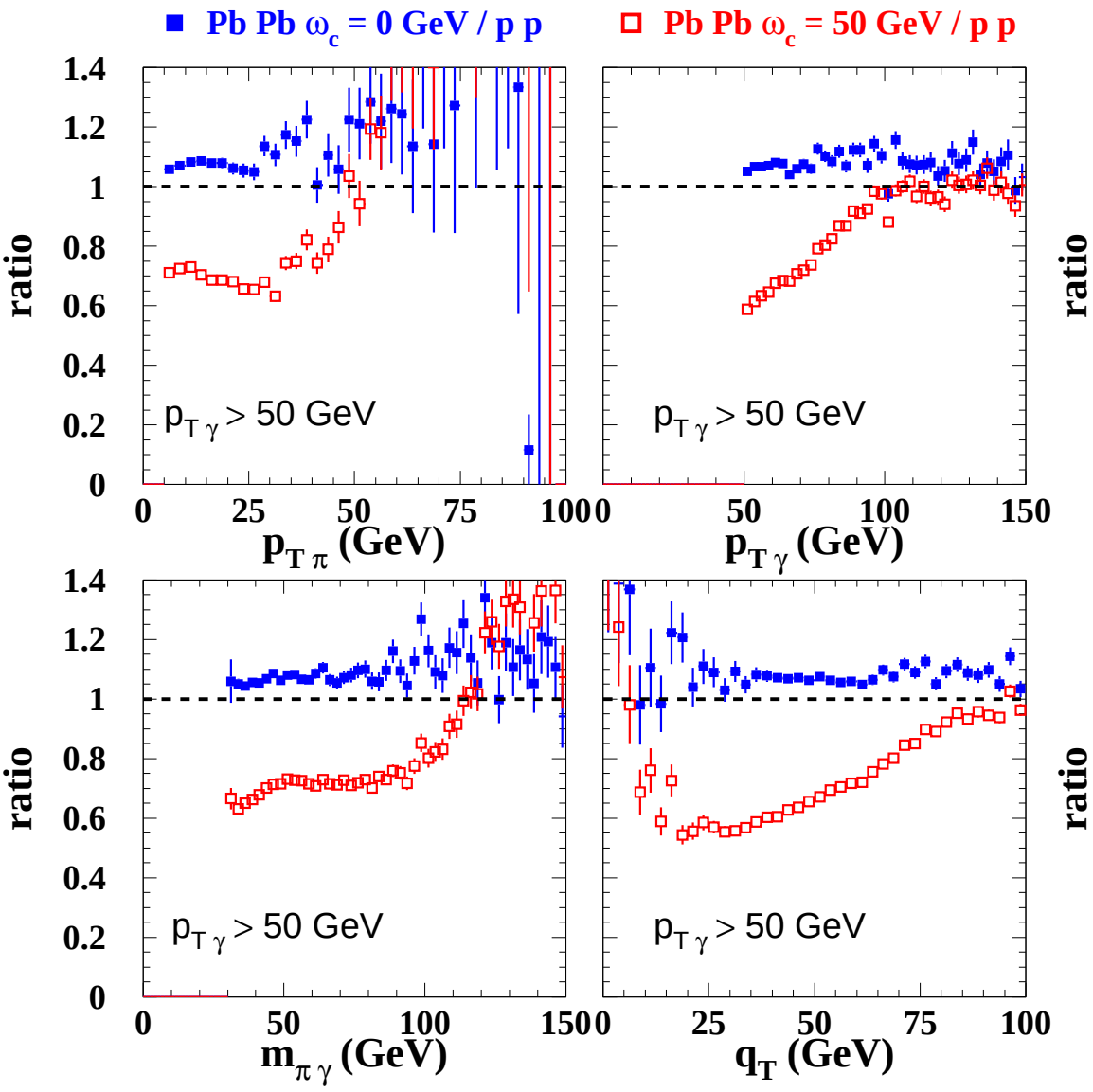

Figure 8: Same as Figure 6 with the following cuts: $p_{T_\gamma} > 50$ GeV and $p_{T_\pi} > 5$ GeV.

would be necessary to increase the photon transverse momentum, making the 2f process highly unlikely. It can be seen from the right panel of Figure 10 that going from a 25 GeV to a 50 GeV p_{T_γ} cut indeed increases significantly the 1f component. Nevertheless, the 2f contribution remains too large at large z_{34} to observe a huge medium suppression in this kinematical region. It may then be necessary to trigger on even more energetic photons, the drawback of too stringent cuts being the smallness of the corresponding cross sections.

As we shall see in the next Section, diphoton production mostly comes from the 1f contribution process at the LHC. This observable may therefore be more interesting than $\gamma - \pi^0$ correlations, at least regarding the momentum imbalance distributions.

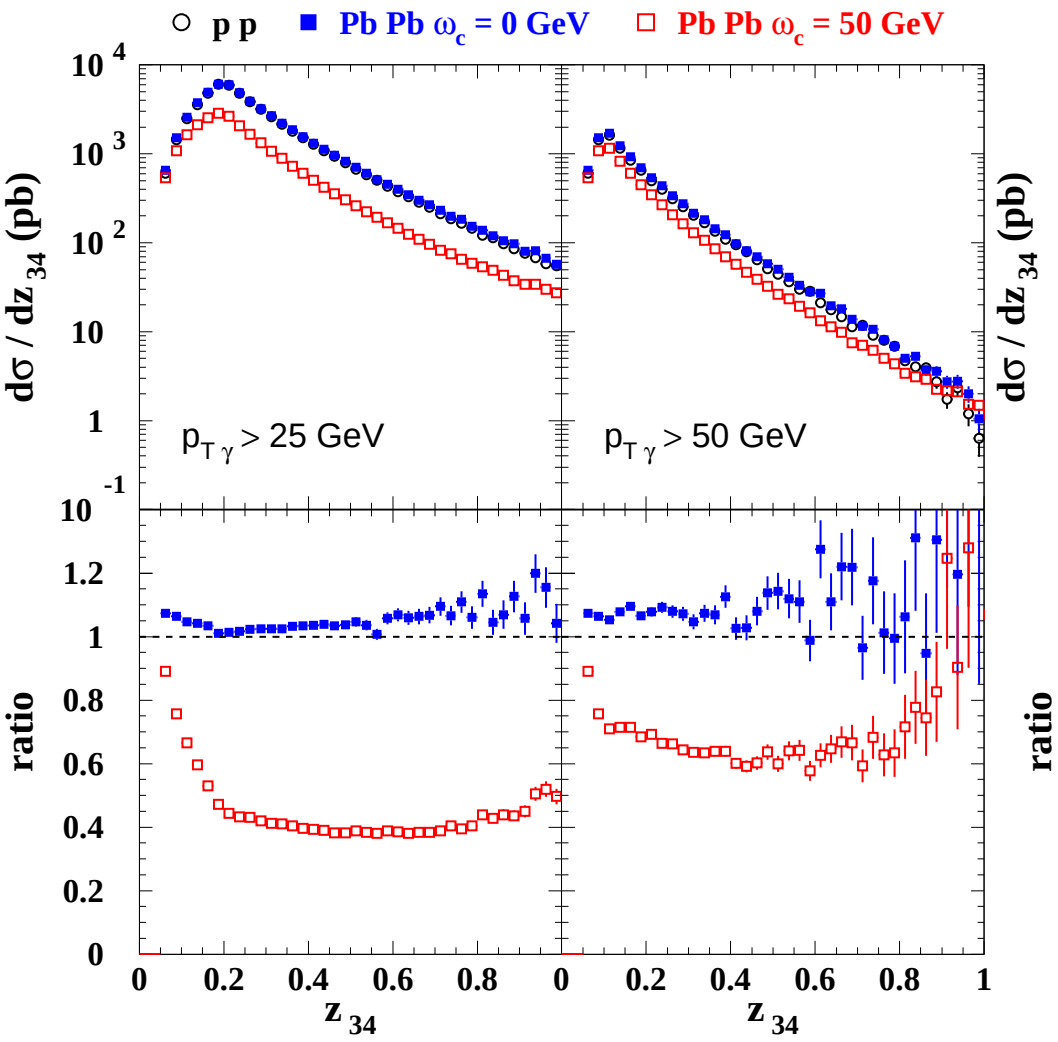

Figure 9: The z_{34} distribution in $\gamma - \pi^0$ production for proton-proton (open dots) and lead-lead scattering (no energy loss: black squares; with energy loss: open squares) at $\sqrt{s} = 5.5$ TeV. Both the photon and the pion are produced at rapidity [-0.5, 0.5] and the following cuts are imposed: $p_{T_\gamma} > 25$ GeV and $p_{T_\pi} > 5$ GeV (*left*) and $p_{T_\gamma} > 50$ GeV and $p_{T_\pi} > 5$ GeV (*right*). *Bottom:* The same distributions normalized to the proton-proton case.

5. Phenomenology of $\gamma - \gamma$ correlations

5.1 Dynamical components

This section is devoted to the study of $\gamma - \gamma$ (or diphoton) correlations in the same kinematic regime as before. As compared to the previous cross sections they are, in principle, a factor $\mathcal{O}(\alpha/\alpha_s)$ smaller, but the counting rates at the LHC should nevertheless remain sufficient for our studies. On top of the 1f and 2f components, the new feature is that both photons can be produced directly (*direct* process, Figure 11) in which case they are not affected by the medium.

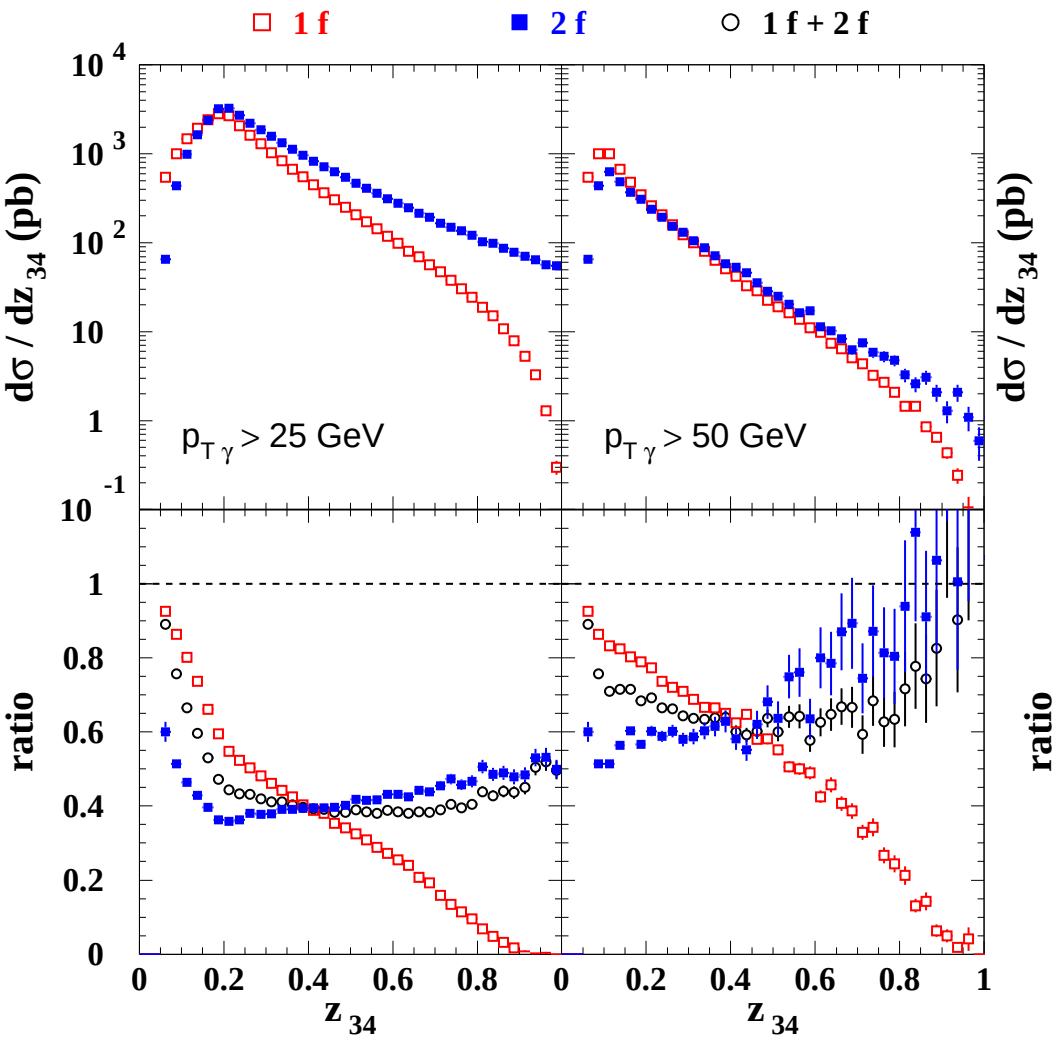

Figure 10: The 1f and 2f components in $\gamma - \pi^0$ production for various kinematical configurations for lead-lead scattering at $\sqrt{s} = 5.5$ TeV. *Top:* The z_{34} distribution for $p_{T_\gamma} >$ 25 GeV (*left*) and $p_{T_\gamma} > 50$ GeV (*right*). *Bottom:* The same distributions normalized to the proton-proton case.

The relative weight of all three components, for proton-proton scattering, are shown in Figure 12 imposing a minimum transverse momentum of 25 GeV on one photon and 5 GeV on the other. We first consider (*top left*) the spectrum in p_{T_γ}. It shows a discontinuity at 25 GeV since below this value only one photon is measured and, furthermore, only the 1f and 2f processes contribute. One observes the dominance of the 1f component for the whole transverse momentum range, even when the direct process contributes, *i.e* above the larger p_{T_γ} cut. Concerning the invariant mass spectrum, the 2f component is at least three times smaller than the 1f contribution, while the direct piece causes a small hump to the total cross section at twice the p_{T_γ} threshold value. Note the "singular" contributions of the direct component at

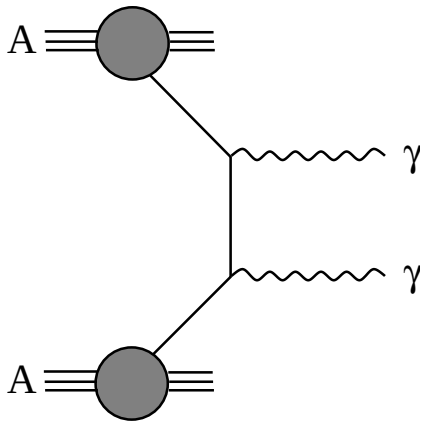

Figure 11: On top of the one-fragmentation and two-fragmentation process, two photons can be produced directly in $\gamma - \gamma$ production at leading order. This process is not affected by the medium and yields singular contributions at $q_{_T} = 0$ GeV and $z_{_{34}} = 1$.

$q_{_T} = 0$ and $z_{_{34}} = 1$, a feature of the leading logarithmic approximation. The ordinate of the corresponding points depend, of course, on the size of the bin (equivalently the resolution of the detector). The shape of the distributions near this infrared singular point is expected to be modified by the higher order corrections.

5.2 Distributions

We now compare in Figure 13 the $p_{_{T_\gamma}}$ and $q_{_T}$ spectra in proton-proton scattering (open dots), lead-lead scattering with shadowing but without energy loss (full squares) and lead-lead scattering with shadowing and energy loss (open squares). The ratios of the lead-lead over proton-proton spectra are also shown. Similarly to the $\gamma - \pi^0$ case, the effects of nuclear shadowing turn out to be negligible. On the contrary, interesting features due to the energy loss mechanism are observed. The strongest suppression of the $p_{_{T_\gamma}}$spectra is reached for transverse momenta of order of the upper cut, $p_{_{T_\gamma}} \simeq 20$ GeV. This can be understood as follows. As $p_{_{T_\gamma}}$ approaches the upper cut from "below", events with larger z are selected, $p_{_{T_{\gamma 2}}} \simeq p_{_{T_{\gamma 1}}}$, where energy loss effects are most pronounced (cf. Figure 2). Above that cut, the proportion of directly produced photons (unaffected by the medium) is getting larger and the quenching factor is slowly reaching unity as expected at asymptotic energies, $p_{_{T_\gamma}} \gg \omega_c$. Looking at the ratio of $q_{_T}$ spectra, the smaller the $q_{_T}$ the larger the suppression of diphoton events in lead−lead collisions. Indeed, since the production is dominated by the 1f process, with $z_3 = 1$, small $q_{_T}$ events imply a large z_4 value for the other photon ($q_{_T} = k_{_T}\ |z_3 - z_4|$) where medium effects are the strongest. Moreover, we no longer observe the same feature as in $\gamma - \pi^0$ production – the mild increase of the ratio at very small $q_{_T}$ (Figure 5, *lower right*) – since the 2f fragmentation contribution to diphoton production is much smaller. Finally, the ratio at

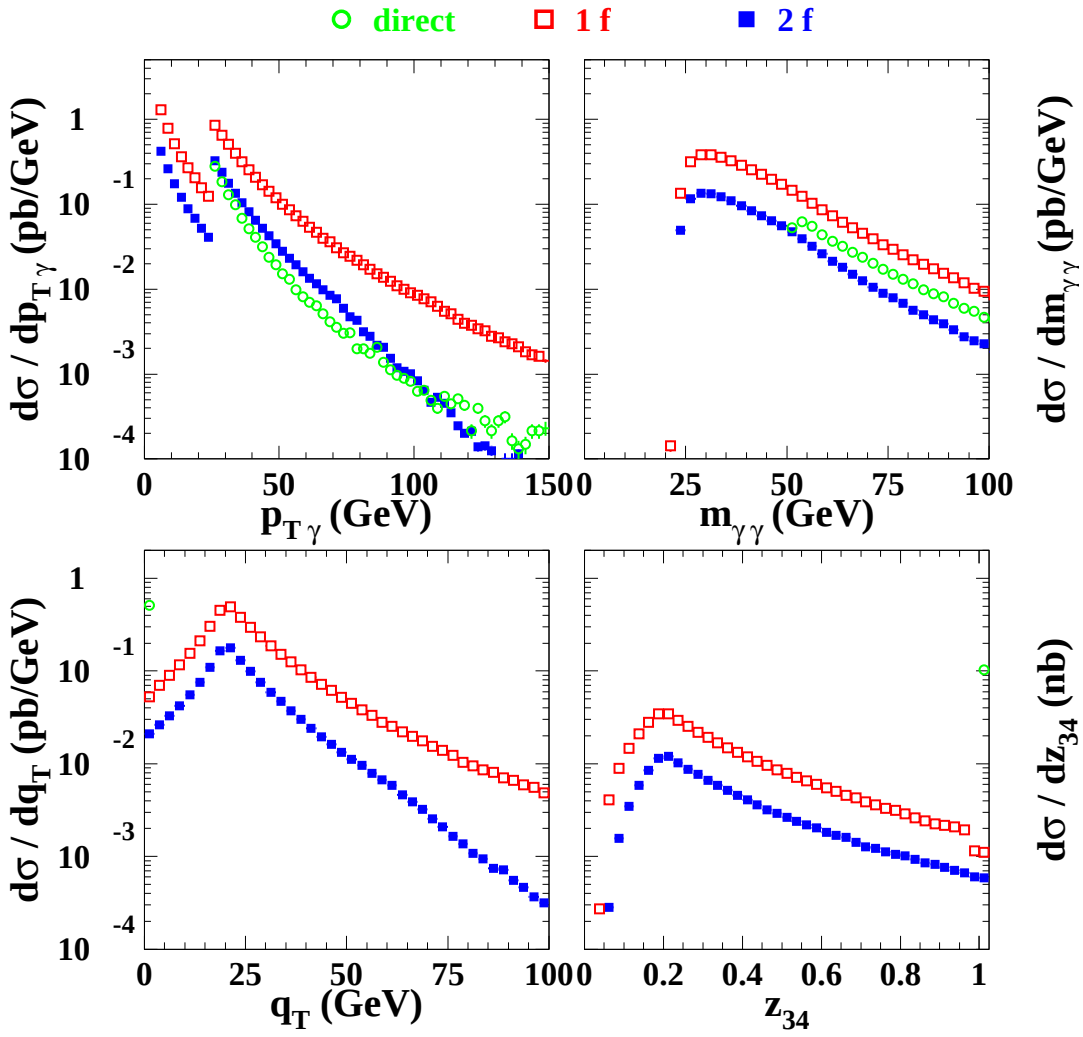

Figure 12: The three components (direct, 1f and 2f) contributing to diphoton production in proton-proton collisions at $\sqrt{s} = 5.5$ TeV. A lower cut of 25 GeV is imposed on the transverse momentum of one photon and 5 GeV on the other. The four distributions shown are in the transverse momentum of either photon, the diphoton invariant mass, the transverse momentum of the pair, the diphoton invariant mass and the momentum imbalance.

$q_T = 0$ GeV is almost close to one due to the singular contribution of the direct process, unaffected by the medium.

The distribution in the diphoton momentum imbalance z_{34} is now discussed in Figure 14, using the previous kinematical cuts $p_{T_{\gamma_1}} \geq 5$ GeV and $p_{T_{\gamma_1}} \geq 25$ GeV (*left*) as well as $p_{T_{\gamma_2}} \geq 5$ GeV and $p_{T_{\gamma_1}} \geq 50$ GeV (*right*) to keep the parallel with Section 4. Similarly to the $\gamma - \pi^0$ distribution, the distribution is maximal around the ratio of the p_{T_γ} cuts ($z_{34} = 0.2$ and 0.1 respectively) and decreases rapidly with z_{34}, a shape reminiscent of the photon fragmentation functions in Figure 2.

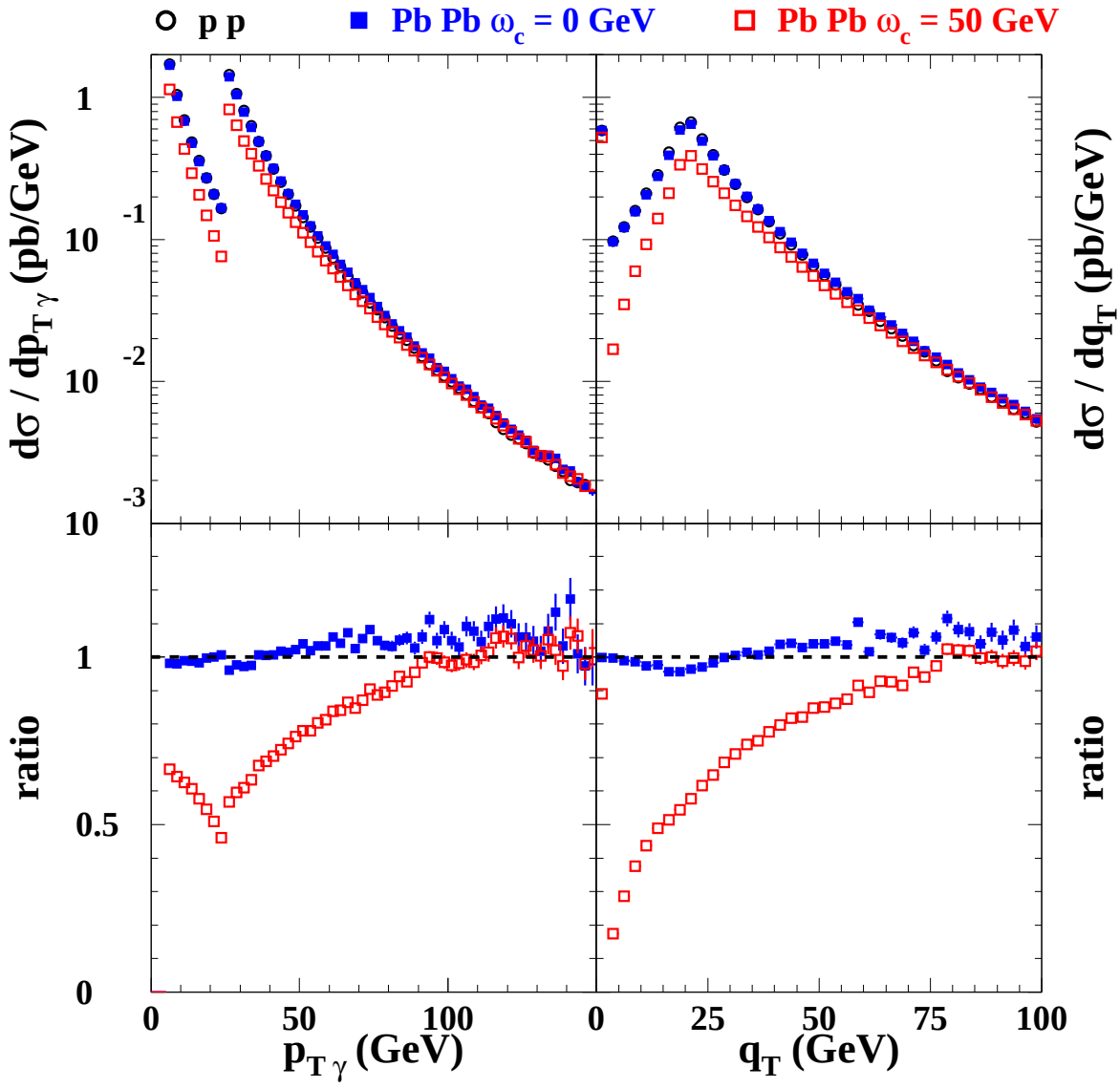

Figure 13: *Top:* The photon p_{T_γ} and photon pair q_T transverse momentum distributions in $\gamma - \gamma$ production for proton-proton (open dots) and lead-lead scattering (no energy loss: black squares; with energy loss: open squares) at $\sqrt{s} = 5.5$ TeV. Both photons are produced at rapidity [-0.5, 0.5] and the following cuts are imposed: $p_{T\gamma_1} > 25$ GeV and $p_{T\gamma_2} > 5$ GeV. *Bottom:* The same distributions normalized to the proton-proton case.

In particular, it is remarkable to notice how the diphoton quenching in Figure 14 (*bottom*, open squares) ressembles the ratio of medium-modified over vacuum parton to photon fragmentation functions (Figure 3). Unlike the $\gamma - \pi^0$ case, the smaller 2f contribution to diphoton production does not spoil too much the large z_{34} suppression and make the interpretation of the momentum imbalance spectra much easier in terms of photon fragmentation functions.

Notice that one expects a reasonable number of photon-photon events: for ex-

ample, for $z_{34} = 0.5$ one has 2 10^4 events for $p_{T_\gamma} > 25$ GeV and 2.5 10^3 for $p_{T_\gamma} > 50$ GeV with ALICE luminosity for one month running time.

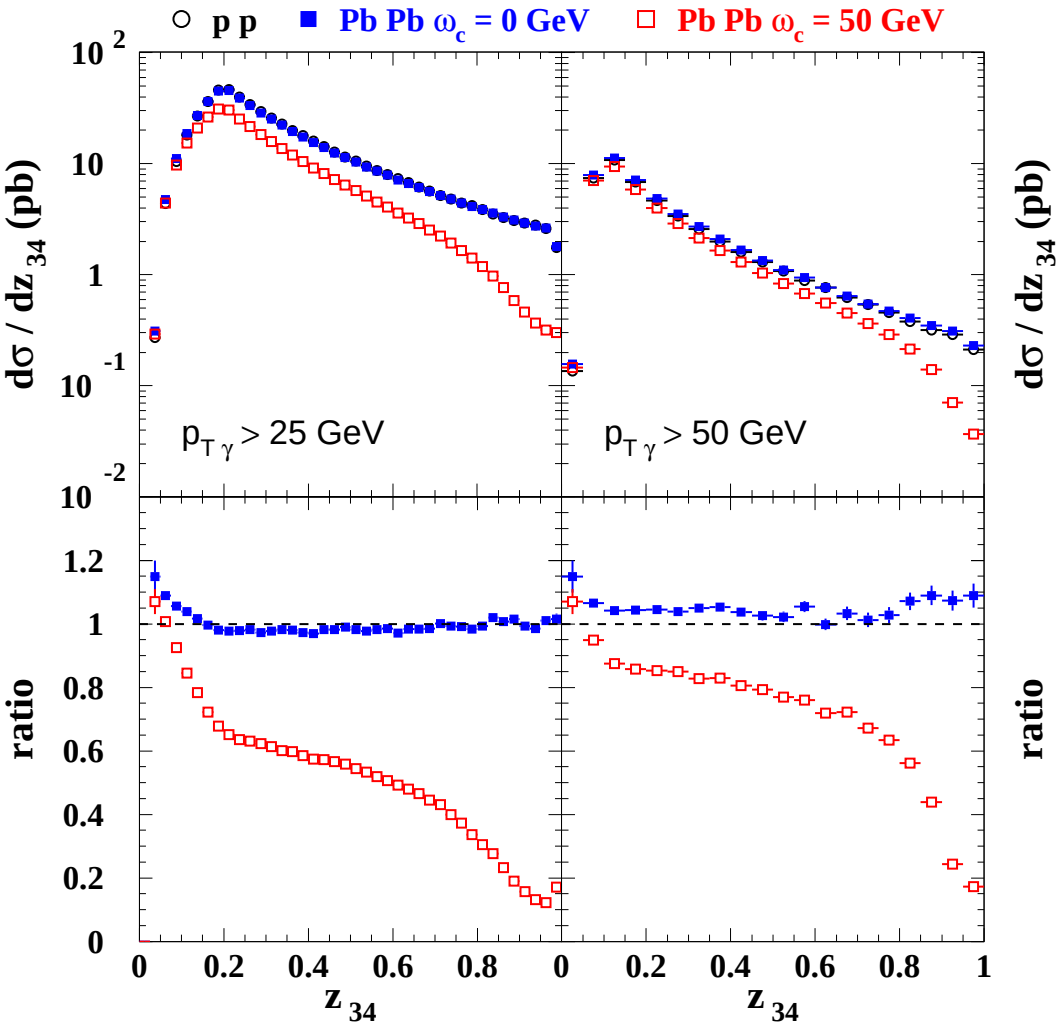

Figure 14: The z_{34} distribution in $\gamma - \gamma$ production for proton-proton (open dots) and lead-lead scattering (no energy loss: black squares; with energy loss: open squares) at $\sqrt{s} = 5.5$ TeV. Both photons produced at rapidity [-0.5, 0.5] and the following cuts are imposed: $p_{T\gamma_1} > 25$ GeV and $p_{T\gamma_2} > 5$ GeV (*left*) and $p_{T\gamma_1} \geq 50$ GeV and $p_{T\gamma_2} \geq 5$ GeV (*right*). *Bottom:* The same distributions normalized to the proton-proton case.

6. Qualitative effects of NLO corrections

As already mentioned, the not yet clarified status of NLO QCD calculations in the medium has lead us to consider $\gamma - \pi^0$ and $\gamma - \gamma$ production to leading order accuracy. Nevertheless, it is instructive to study and quantify the role of higher order corrections in proton-proton collisions. In particular, attention should be paid to the

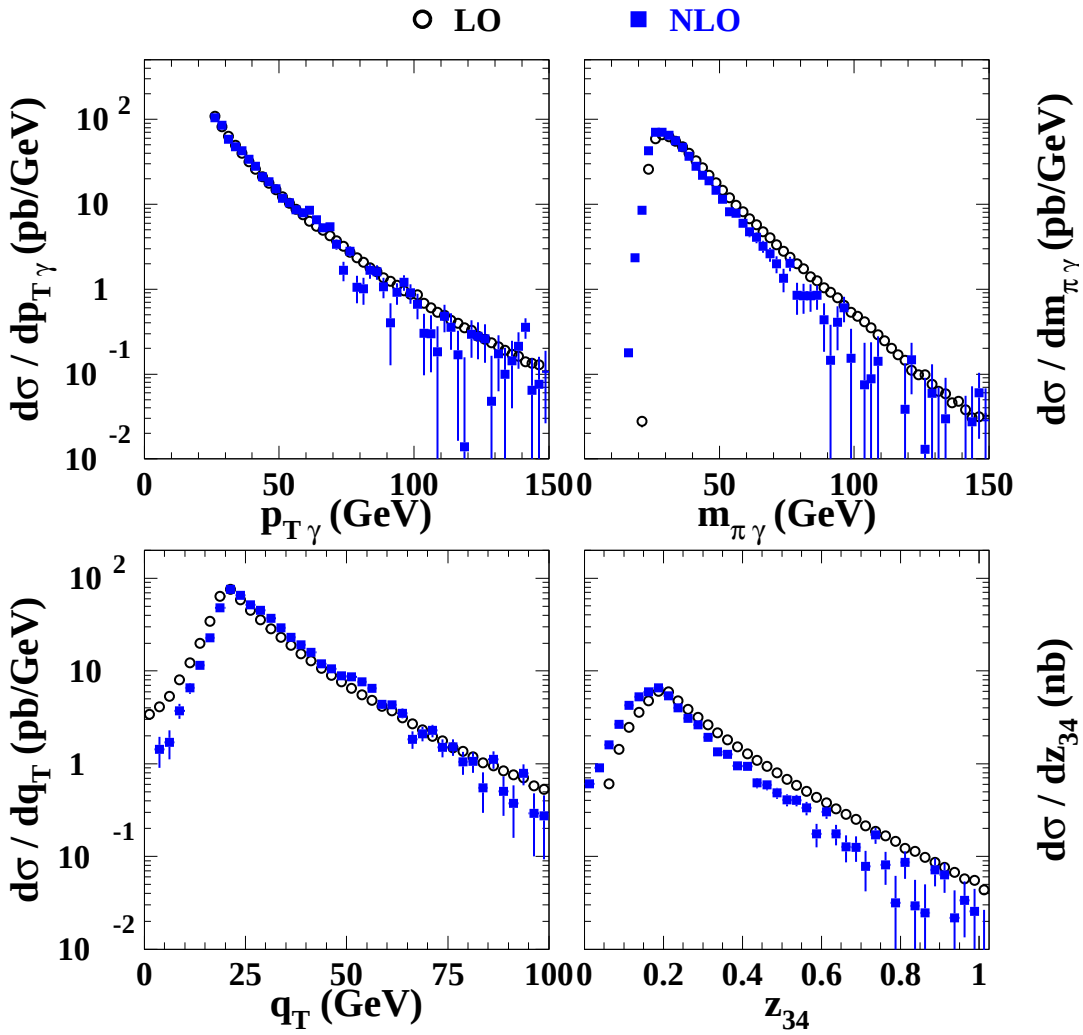

Figure 15: Comparison of LO and NLO calculations for various $\pi - \gamma$ correlations.

phase space which gets modified by higher order QCD corrections: consequently this can affect our leading order predictions in lead-lead collisions.

The NLO predictions are obtained using the CTEQ6M structure functions [13], the KKP next-to-leading logarithmic fragmentation functions for the π^0 and the BFG, set II, fragmentation functions into a photon. As before all scales are set equal to $(p_{_{T_3}} + p_{_{T4}})/2$. A cut in the azimuthal angle between the two particles has been applied, $\phi \geq \phi_{\rm min} = \pi/2$.

The $\gamma - \pi^0$ correlation functions are plotted in Figure 15 at LO (*dots*) and NLO (*squares*). The overall effect of higher order corrections proves quite small – say less than 30 % – except in some specific regions of phase space. As shown in Figure 16, the ratio of NLO over LO spectra is almost constant except at small invariant mass or momentum imbalance. The reason comes from the new parton configurations in momentum space available at higher order. Indeed, the two particles are no longer

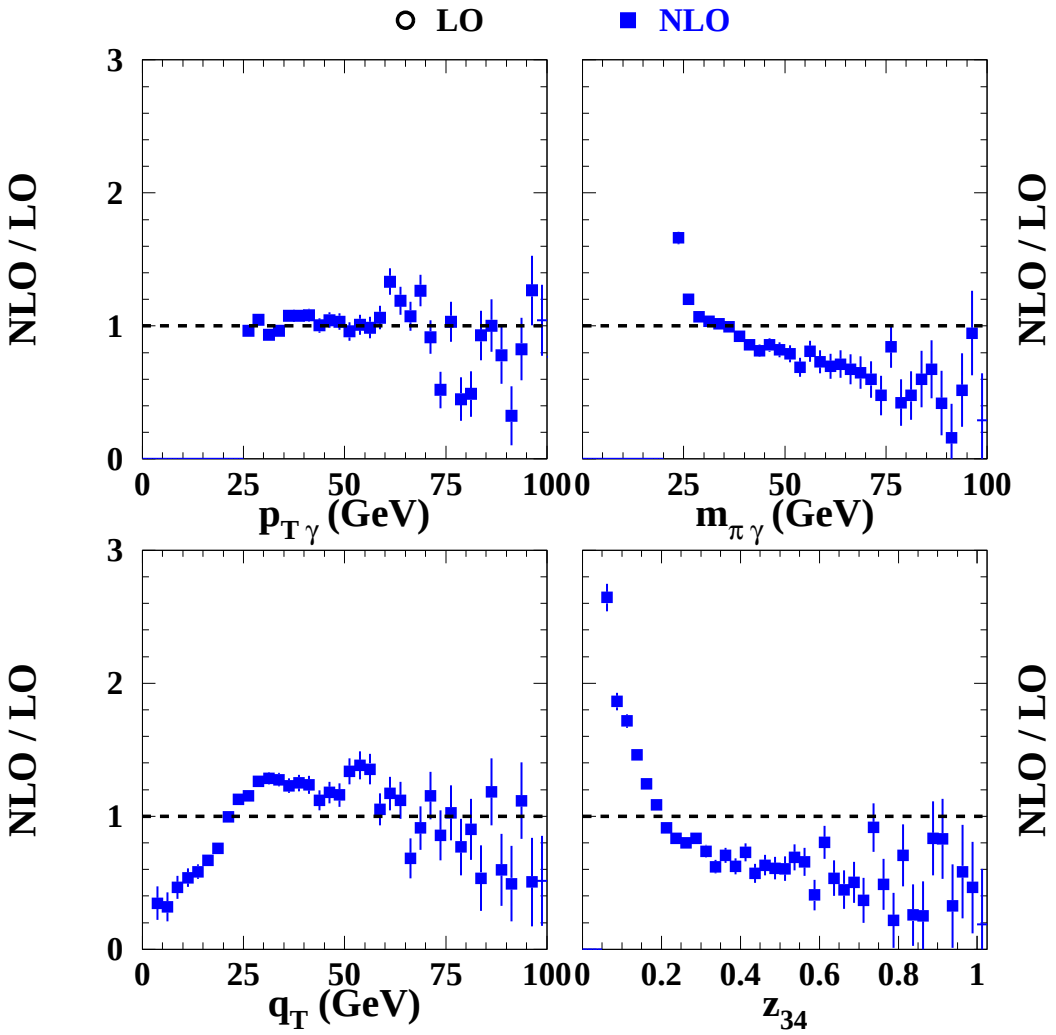

Figure 16: Ratio of NLO over LO estimates of the $\pi - \gamma$ correlations shown in Figure 5.

constrained to have opposite momenta when going from the two-body to the three-body NLO kinematics. This will affect, in particular, variables like the invariant mass, the pair transverse momentum or the momentum imbalance which now depend explicitely on the relative azimuthal angle ϕ between the two particles (see Eqs. (3.1) to (3.3)). This can be seen in Figure 16 where the momentum imbalance spectrum is clearly enhanced at NLO when $z_{34} \propto \cos\phi$ gets very small: this corresponds to configurations where the observed particles are recoiling from the third undetected jet in the opposite hemispere. Other effects include the shift of the threshold in the invariant mass distribution, from $m_{\pi\gamma} = \sqrt{4p_{T_\gamma}p_{T_\pi}} = 10\sqrt{5}$ GeV ($\phi = \pi$) to $m_{\pi\gamma} = \sqrt{2p_{T_\gamma}p_{T_\pi}} = 5\sqrt{10}$ GeV ($\phi = \pi/2$), or the shift of the pair momentum spectrum to larger q_T which results in the ratio smaller than one below 20 GeV (the difference of the p_T cuts, i.e. the maximum of the distribution) and larger above. All these effects depend crucially on the cut $\phi_{\rm min}$ in the azimuthal angle and should

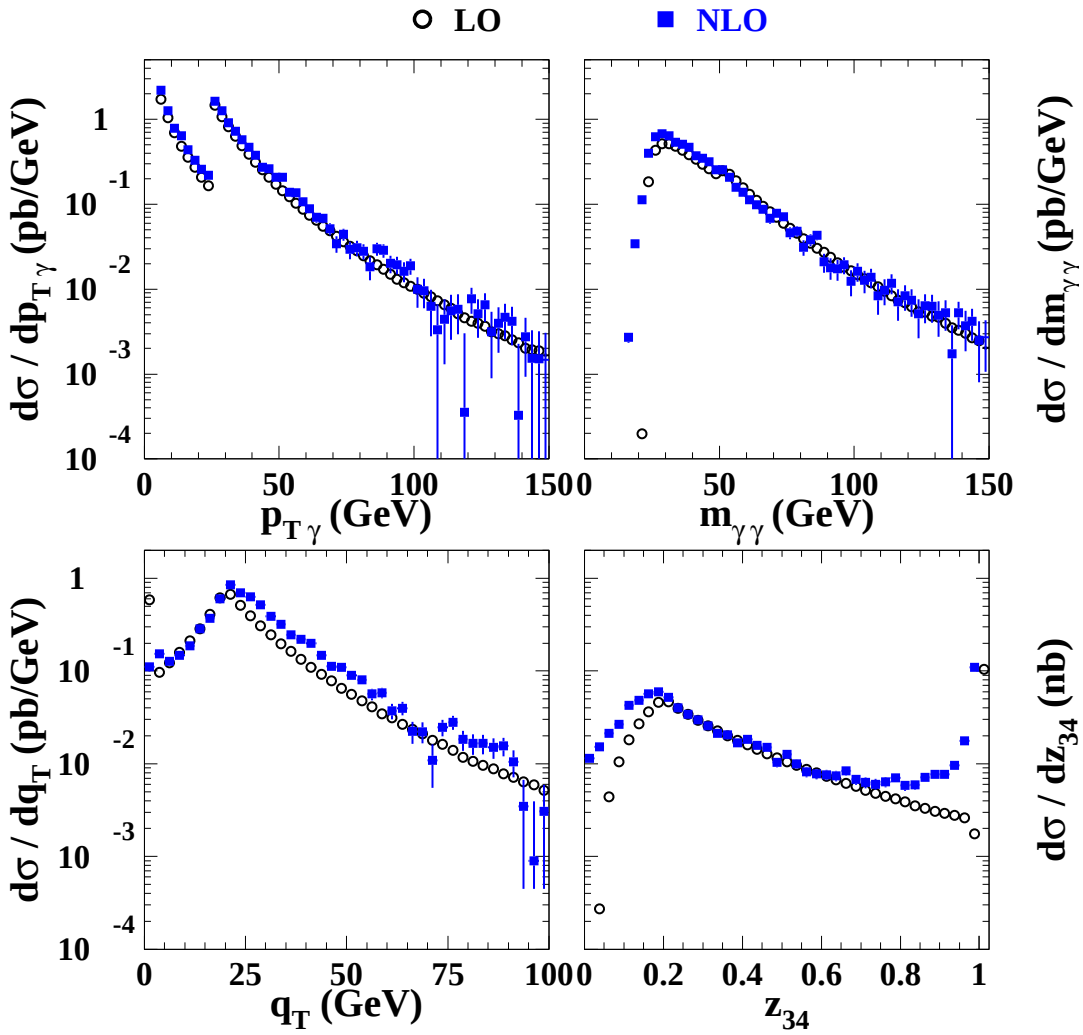

Figure 17: The NLO correlations in $\gamma - \gamma$ production for proton-proton scattering at $\sqrt{s} = 5.5$ TeV.

vanish as $\phi_{\rm min}$ approaches π.

The $\gamma - \gamma$ correlation functions displayed in Figure 17 indicate that higher order corrections do not strongly modify the LO results in this channel either, except near the infrared singular point ($q_{_T} = 0$ GeV or $z_{_{34}} = 1$) or in the domain where new phase space is available (small $m_{_{\gamma\gamma}}$ or small $z_{_{34}}$). In the latter case the NLO momentum configurations modify the LO spectra in a way similar to the $\gamma - \pi^0$ correlations (see the spectrum ratios in Figure 18). Although the effect proves tiny, we may also remark the lower threshold for the direct process in the transverse momentum distribution, now slightly below the 25 GeV cut. However, the most remarkable feature when going from LO to NLO in $\gamma - \gamma$ production deals with the infrared sensitivity of observables such as the transverse momentum or the momentum imbalance spectrum. When $q_{_T}$ gets small as compared to the diphoton invariant mass, the phase

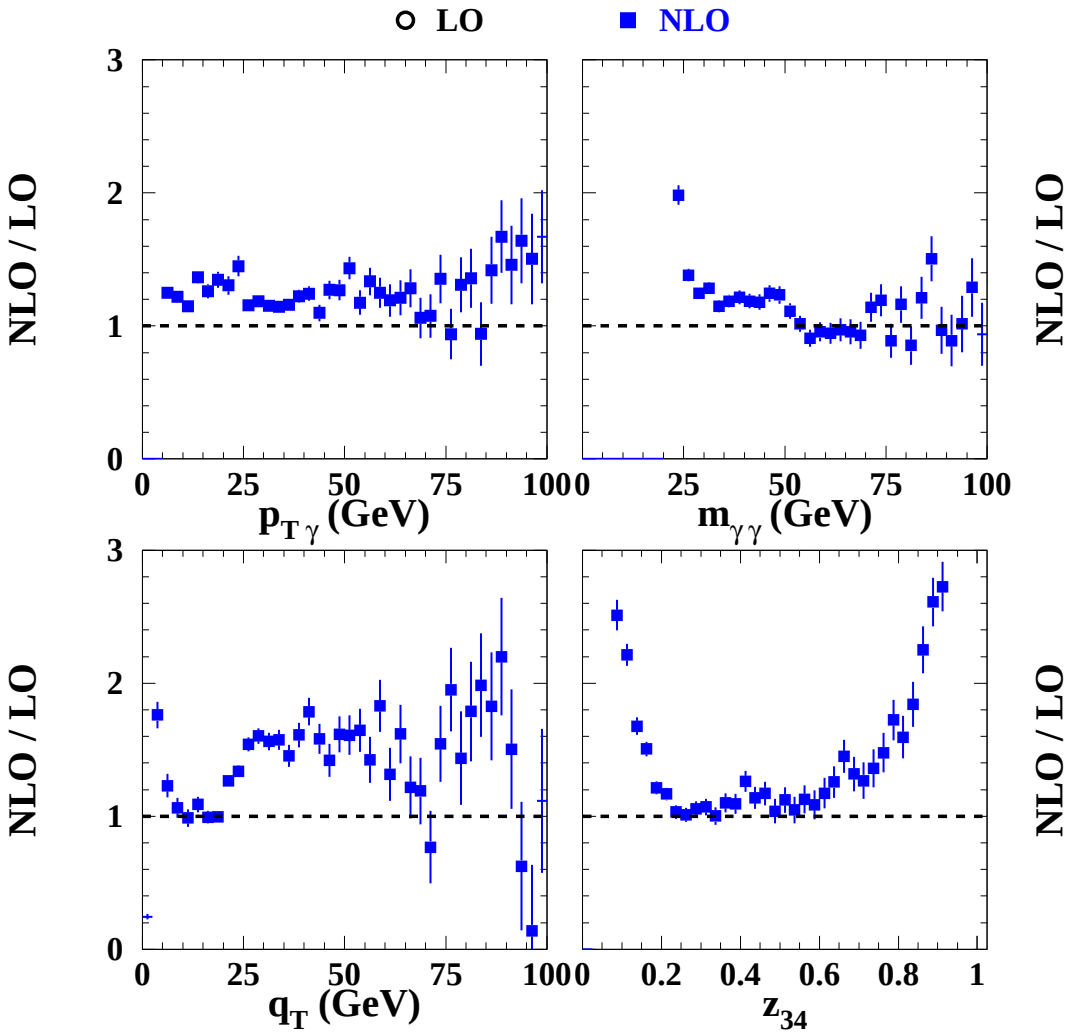

Figure 18: Ratio of NLO correlations over LO correlations for $\gamma - \gamma$ production. See Figure. 17 for details.

space restriction forces the emitted gluons to be extremely soft. The δ function singularity which appeared in the leading logarithm approximation now spreads in phase space, due to the partial cancellation of real and virtual NLO terms, and it is broadened at NLO accuracy. Indeed, we notice in Figure 17 the significant corrections which extend up to roughly $q_{_T} \lesssim 10$ GeV. This gives us a typical range in which the present perturbative calculation may not be reliable. Since $q_{_T}/m_{\gamma\gamma} \propto 1 - z_{34}$, such a behavior can also be observed in the momentum imbalance spectrum near the singular point, $z_{34} = 1$ where the NLO results start to deviate significantly from the LO prediction above $z_{34} \gtrsim 0.8$. Technically, large terms such as $\alpha_s \ln^2\left(q_{_T}^2/m_{\gamma\gamma}^2\right)$ and $\alpha_s \ln\left(q_{_T}^2/m_{\gamma\gamma}^2\right)$ contribute to the direct process making the present fixed order QCD calculation not reliable very near the infrared singular point. For a more accurate approximation such large terms should be resummed. Although the one (two) frag-

mentation component requires one (two) integration(s) over the scaling variable z_3 (z_3 and z_4), which smears out these large logarithms [7] and make the distributions regular at small q_T, resummation may affect the shape of the distributions in this region.

Let us now discuss the phenomenological implications of higher order corrections to our predictions for the spectrum ratios in lead-lead over those in proton-proton collisions. First the moderate higher order corrections (except in specific domains for some correlations) clearly indicate that neither the absolute attenuation nor the shape of the attenuation in lead-lead collision should be affected too much. In fact, the larger presence of gluons at higher order, whose energy loss is stronger than for quarks, should be responsible for a slightly more pronounced suppression. In the large q_T or small z_{34} region, where the NLO over LO ratio is the largest due to the non-collinear configurations, one can also expect the quenching to prove more pronounced. Indeed, such regions were not affected much by the medium in our LO prediction as they require the fragmentation of very large k_T partons, hence with a small energy loss effect. At NLO, however, the large q_T and small z_{34} domain can be reached while keeping the parton energy k_T not too large (as compared to ω_c), provided the relative azimuthal angle between the two particles is small enough.

We emphasized in the previous section the strong attenuation of diphoton production expected in lead-lead collision near the boundary of phase space, in particular at large z_{34} and small q_T. On the other hand, the presence of the direct process, unaffected by parton energy loss, should make the ratio equal to one exactly at $z_{34} = 1$ and $q_T = 0$ GeV. The competition between the direct and the fragmentation process at LO therefore generated discontinuities in the ratio at these specific points (see e.g. Figure 13), which should be smoothed at higher order. Based on the present NLO calculation in proton-proton reactions, we expect that the quenching of diphoton production should start to increase below $q_T \lesssim 10$ GeV or $z_{34} \gtrsim 0.8$. Similarly, the discontinuity seen in Figure 13 for 25 GeV photon transverse momenta should be smeared as well.

7. Background

In the photon transverse momentum range discussed above the background from π^0 decays will still be appreciable. In order to illustrate this background we briefly present here various $\pi^0-\pi^0$ distributions, using the same asymmetrical cuts as before, namely $p_{T_{\pi_1}} > 25$ GeV and $p_{T_{\pi_2}} > 5$ GeV (see Figure 19). In this case only the 2f mechanism contributes and, as a consequence, the distributions display very similar features to the $\gamma - \pi^0$ case. Only the size of the correlations is larger by roughly a factor 50. Such distributions should therefore be determined with a great accuracy to be subtracted in order to measure the $\gamma - \pi^0$ and $\gamma - \gamma$ distributions discussed so far.

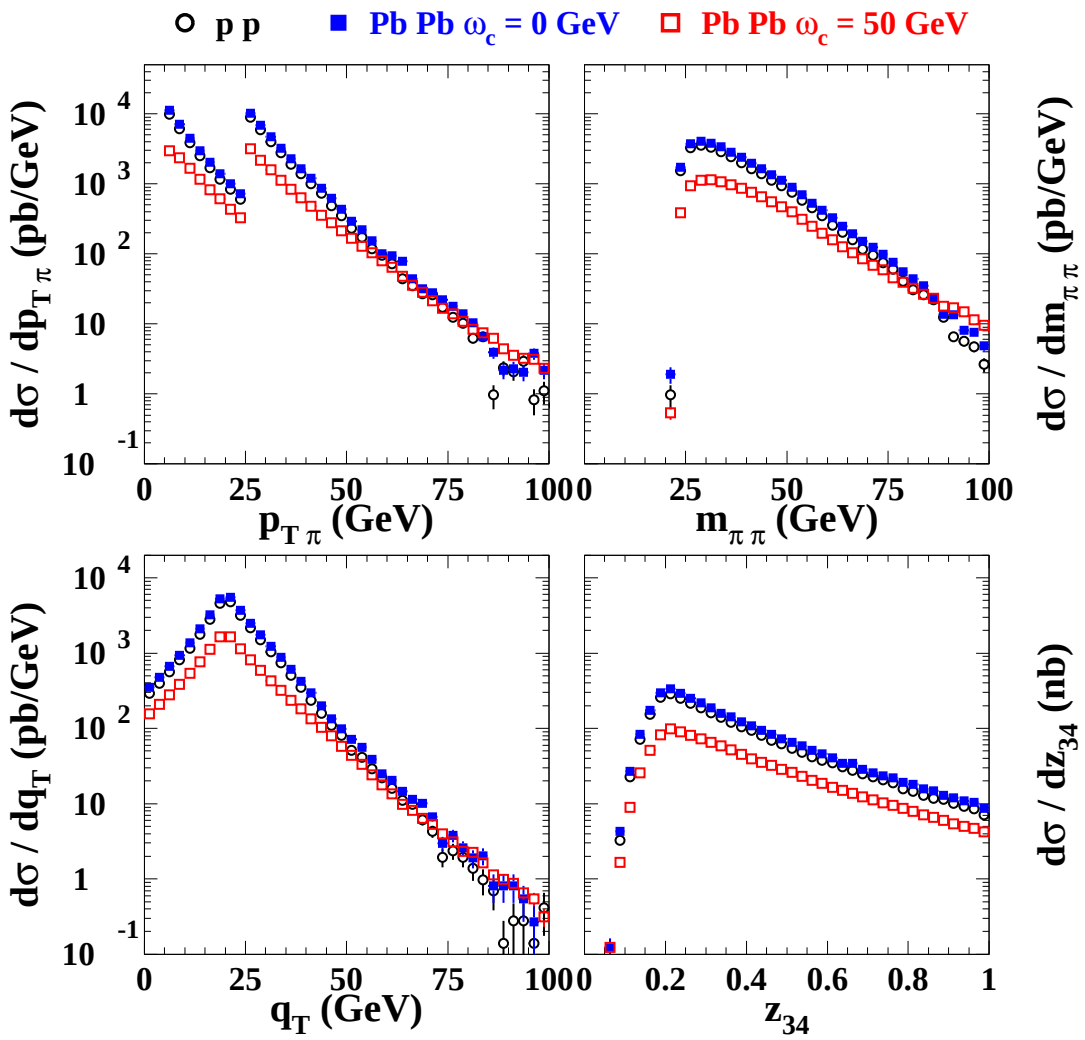

Figure 19: $\pi^0 - \pi^0$ correlations. Both pions are produced at rapidity [-0.5, 0.5] and the following cuts are imposed: $p_{T\pi_1} > 25$ GeV and $p_{T\pi_2} > 5$ GeV. The conventions for the symbols are as in Figure 5.

Although one may still notice significant effects in nucleus-nucleus collisions, medium-modified fragmentation functions cannot be determined through $\pi^0 - \pi^0$ correlations in the absence of the 1f component. Nevertheless, we feel it should be interesting to perform such correlations with low p_{T_π} cuts for *both* pions which would possibly allow to study the spatial distribution of the hot medium. This has been achieved for instance by the RHIC experiments who considered the $\pi^0 - \pi^0$ azimuthal correlations [36]. Theoretically, this would require a complete description of the space-time energy density though – available e.g. in hydrodynamical models – which go beyond the scope of the present study. Such attempts have been suggested recently [28, 29].

8. Conclusions

We have discussed various photon tagged correlations as a tool to study jet fragmentation in the hot medium created in heavy-ion collisions. Correlations functions have been computed to leading order in proton-proton collisions at LHC energy. Similar distributions were determined in lead-lead collisions, assuming medium-modified fragmentation functions to account for the parton energy loss process in the dense medium.

We show that significant effects could be expected at LHC energy both in the $\gamma-\pi^0$ and $\gamma-\gamma$ channel. Ideally, the use of asymmetric cuts in the transverse momentum of both particles allow the possibility to map out the parton fragmentation functions modified by the medium. However several production mechanisms co-exist with a relative weight varying with the kinematical variable under consideration. This smears somehow the relation between observables and the fragmentation functions. Consequently, we found various suppression patterns, depending on the imposed kinematical constraints, which should be accessible experimentally. Furthermore, the variety of observables presented here should help to constrain the underlying model for parton energy loss.

Although calculations were performed at leading order, NLO corrections have also been addressed. In particular, the way higher order corrections could modify the expected quenching of $\gamma-\pi^0$ and $\gamma-\gamma$ spectra is discussed. To be more specific, we believe our present LO prediction to be reliable up to roughly $z_{_{34}} \simeq 0.8$. Finally, $\pi^0-\pi^0$ correlation functions were computed so as to give a reference for the expected background one could face at the LHC within the kinematic cuts we employed.

Acknowledgments

The authors thank Hugues Delagrange and Monique Werlen for discussions.

References

[1] WA98 Collaboration, M.M. Aggarwal *et al.*, Phys. Rev. Lett. **85**, 3595 (2000).

[2] Jan-e Alam, S. Sarkar, T. Hatsuda, T. K. Nayak, B. Sinha, Phys. Rev. **C63**, 021901 (2001)
D. K. Srivastava, B. Sinha, Phys. Rev. **C64**, 034902 (2001);
A.K. Chaudhuri, J. Phys. G **29**, 235 (2003).

[3] P. Huovinen, P.V. Ruuskanen, S.S. Räsänen, Phys .Lett. **B535**, 109 (2002).

[4] F. Arleo *et al.*, *Photon Physics in Heavy Ion Collisions at the LHC* , CERN Yellow report on *Hard probes in Heavy Ion collisions at the LHC*, hep-ph/0311131.

[5] P. Aurenche, P. Chiappetta, M. Fontannaz, J.-Ph. Guillet, E. Pilon, Nucl. Phys. **B399**, 34 (1993).

[6] P. Chiappetta, R. Fergani, J.-Ph. Guillet, Z. Phys. **C69**, 443 (1996).

[7] T. Binoth, J.-Ph. Guillet, E. Pilon, M. Werlen, Eur. Phys. J. **C16**, 311 (2000); Phys Rev. **D63**, 114016 (2001); EPJdirect **C4**, 7 (2002).

[8] J.-Ph. Guillet *el al.*: the DIPHOX code upon which these studies are based can be found at `http://wwwlapp.in2p3.fr/lapth/PHOX_FAMILY/diphox.html`.

[9] X.-N. Wang, Z. Huang, I. Sarcevic, Phys. Rev. Lett. **77**, 231 (1996); X.-N. Wang, Z. Huang, Phys. Rev. **C55**, 3047 (1997).

[10] J. Jalilian-Marian, K. Orginos, I. Sarcevic, Phys. Rev. **C63**, 041901 (2001); Nucl. Phys. **A700**, 523 (2002); S. Jeon, J. Jalilian-Marian, I. Sarcevic, Phys. Lett. **B562**, 45 (2003).

[11] B.A. Kniehl, G. Kramer, B. Potter, Nucl. Phys. **B582**, 514 (2000).

[12] L. Bourhis, M. Fontannaz, J.-Ph. Guillet, Eur. Phys. J. **C2**, 529 (1998).

[13] J. Pumplin, D.R. Stump, J. Huston, H.L. Lai, P. Nadolsky, W.K. Tung, JHEP **0207**, 012 (2002).

[14] WA70 collaboration, E. Bonvin *et al.*, Phys. Lett. **B236**, 523 (1990).

[15] E706 Collaboration, L. Apanasevich *et al.*, Phys. Rev. Lett. **81**, 2642 (1998).

[16] D0 collaboration, P. Hanlet, Nucl. Phys. **B64** (Proc. Suppl), 78 (1998); B. Abbot *et al.*, Phys. Rev. Lett. **86**, 1156 (2001).

[17] M.R. Adams *et al.*, Phys. Rev. Lett. **68**, 3266 (1992).

[18] E772 collaboration, D.M. Alde *et al.*, Phys. Rev. Lett. **64**, 2479 (1990); E866/NuSea collaboration, M.A. Vasiliev *et al.*, Phys. Rev. Lett. **83**, 2304 (1999).

[19] K.J. Eskola, V.J. Kolhinen, C.A. Salgado, Eur. Phys. J. C **C9**, 61 (1999).

[20] A. Accardi *et al.*, *PDF, shadowing and pA collisions*, CERN Yellow report on *Hard probes in Heavy Ion collisions at the LHC*, hep-ph/0308248.

[21] For reviews, see R. Baier, D. Schiff, B.G. Zakharov, Ann. Rev. Nucl. Part. Sci. **50**, 37 (2000); M. Gyulassy, I. Vitev, X.-N. Wang, B.-W. Zhang, published in Hwa, R.C. (ed.) et al. "Quark-Gluon Plasma 3", pp. 123-191; I. Vitev, J. Phys. **G30**, S791 (2004).

[22] R. Baier, Yu.L. Dokshitzer, A.H. Mueller, D. Schiff, JHEP **0109**, 033 (2001).

[23] F. Arleo, JHEP **0211**, 044 (2002).

[24] C.A. Salgado, U.A. Wiedemann, Phys. Rev. **D68**, 014008 (2003).

[25] R. Baier, Yu.L. Dokshitzer, A.H. Mueller, S. Peigné, D. Schiff, Nucl. Phys. **B484**, 265 (1997).

[26] R. Baier, Yu.L. Dokshitzer, A.H. Mueller, D. Schiff, Nucl. Phys. **B531**, 403 (1998).

[27] F. Arleo, Eur. Phys. J. **C30**, 213 (2003).

[28] K.J. Eskola, H. Honkanen, C.A. Salgado, U.A. Wiedemann, hep-ph/0406319.

[29] A. Dainese, C. Loizides, G. Paic, hep-ph/0406201.

[30] R. Baier, Yu.L. Dokshitzer, A.H. Mueller, S. Peigné, D. Schiff, Nucl. Phys. **B483**, 291 (1997).

[31] C.A. Salgado, U.A. Wiedemann, Phys. Rev. Lett. **89**, 092303 (2002).

[32] K.J. Eskola, H. Niemi, P.V. Ruuskanen, S.S. Räsänen, private communication.

[33] N. Armesto, C. Pajares, Int. J. Mod. Phys. **A15**, 2019 (2000).

[34] F. Arleo, Proceedings 39th Rencontres de Moriond on QCD and High-Energy Hadronic Interactions, hep-ph/0406291.

[35] P. Aurenche, R. Baier, A. Douiri, M. Fontannaz, D. Schiff, Z. Phys. **C28**, 309 (1984).

[36] STAR Collaboration, C. Adler *et al.*, Phys. Rev. Lett. **90**, 032301 (2003); C. Adler *et al.*, Phys. Rev. Lett. **90**, 082302 (2003).